Mineralium Deposita (2022) 57:1449–1468
https://doi.org/10.1007/s00126-022-01114-2

ARTICLE

# Genesis of the Maogongdong deposit in the Dahutang W-Cu-(Mo) ore field of northern Jiangxi Province, South China: constraints from mineralogy, fluid inclusions, and H-O-C-S isotopes

Da-Long Hu[1] · Shao-Yong Jiang[1,2] · Suo-Fei Xiong[2] · Jia-Xiang Dong[1] · Ke-Xin Wang[1]

Received: 12 April 2021 / Accepted: 6 April 2022 / Published online: 29 April 2022


## Abstract

The Maogongdong deposit is located in the giant Dahutang W-Cu-(Mo) ore field, northern Jiangxi Province, South China. It is mainly a vein-type deposit, characterized by early W and late Cu-Mo mineralization, and temporally and spatially associated with Late Mesozoic S-type muscovite granites emplaced into a Neoproterozoic granodiorite batholith and the Shuangqiaoshan Group metasedimentary rocks. Fluid inclusions and H–O isotopes suggest that the early ore-forming fluids of the Maogongdong deposit are mainly magmatic water with relatively high temperature (270–410 °C) and moderate-to-low salinity, while the late ore-forming fluids are mixed with meteoric water, with medium-to-low temperature (160–270 °C) and low salinity. Infrared and conventional microthermometric studies of fluid inclusions of the main tungsten mineralization stage show that the homogenization temperatures of primary fluid inclusion assemblages in wolframite (325 to 355 °C) are about 20 °C higher than those of coexisting scheelite and generally 40 °C higher than those in quartz. The $\delta^{34}S$ values of sulfides (− 5.2 to − 1.3 ‰) in the sulfide stage are slightly lower than the magmatic sulfur (− 1.7 to 0.6 ‰) in the pre-ore stage, most likely due to an increase in oxygen fugacity. The low carbon isotope values (− 26.2 to − 15.5 ‰) of fluid inclusions in the tungsten mineralization stage show that a large amount of organic carbon was added before mineralization. Fluid cooling and pressure decrease are the main factors of tungsten ore precipitation, while local boiling may also make a contribution. Mixing of the different fluids led to the formation of copper and molybdenum ores.

**Keywords** Maogongdong · Dahutang · Fluid inclusion assemblages · H-O-C-S Isotopes · Wolframite

## Introduction

South China is one of the most important tungsten provinces in the world, with the largest resources and comprehensive ore deposit types (Chen et al. 2008, 2013; Mao et al. 2013; Xia et al. 2018). Tungsten deposits are mainly distributed in the Nanling tungsten–tin metallogenic belt and the northern Jiangxi–southern Anhui tungsten metallogenic belt, characterized by large total reserves (over 6 million tonnes $WO_3$, Jiang et al. 2020) and the development of super-large ore deposits (e.g., Dahutang, Zhuxi; Mao et al. 2020).

The giant Dahutang W-Cu-(Mo) ore field is located in the eastern part of the Jiangnan orogenic belt of the northern Jiangxi–southern Anhui tungsten metallogenic belt, which is among the largest ones in China and perhaps in the world, with established resources of 2 Mt (million tonnes) $WO_3$, 0.65 Mt Cu, and 0.08 Mt Mo (Jiang et al. 2015). It is characterized by quartz-vein-type wolframite, altered-granite-type scheelite, and the coexistence of tungsten and copper.

So far, most research has been focused on geological features and mineral prospects (Lin et al. 2006; Xiang et al. 2012, 2013; Zuo et al. 2014; Jiang et al. 2015; Fan et al. 2019), geochronology, geochemistry of ore-related granites (Huang and Jiang, 2013, 2014; Mao et al. 2013, 2015; Feng et al. 2012; Xiang et al. 2013; Wei et al. 2018; Fan et al. 2019), and mineralogy (Sun and Chen 2017; Sun et al. 2018; Hu and Jiang, 2020; Fan et al. 2020). However, origin and

Editorial handling: R. Hu

✉ Shao-Yong Jiang
shyjiang@cug.edu.cn

[1] State Key Laboratory of Geological Processes and Mineral Resources, School of Earth Resources, China University of Geosciences, Wuhan 430074, People's Republic of China

[2] Collaborative Innovation Center for Exploration of Strategic Mineral Resources, China University of Geosciences, Wuhan 430074, People's Republic of China

evolution of the ore fluids have attracted much less attention in this ore district. Despite many papers published (e.g., Gong et al. 2015; Ye et al. 2017; Song et al. 2018a; Peng et al. 2018; Zhang et al. 2019), there is still many doubt on the fluid evolution and metal sources, especially the formation temperature and pressure of ore minerals. More systematic studies on fluid inclusions need to be carried out.

Here we present a systematic investigation of the Maogongdong deposit, which is a newly discovered small-sized deposit in the southeastern part of the Dahutang W-Cu-(Mo) ore field (Fig. 1). The geological background of the Maogongdong deposit is similar to the large Shiweidong deposit in the southern part of the district. Our study includes (1) petrographic observation, (2) infrared and conventional microthermometric measurements of fluid inclusions in both ore minerals and gangue minerals at different ore stages, (3) laser Raman and H-O-C isotope analyses of fluid inclusions, (4) in situ sulfur isotope analysis, (5) comparison of major elements of wolframite with different occurrences, in an attempt to: (1) reveal the origin and P-T-S-ρ (pressure, temperature, salinity, density) evolution of ore-forming fluids; (2) indicate the source of ore-forming materials; (3) summarize the ore genesis and clarify the metallogenic process of the Maogongdong deposit.

## Geological background

### Geological setting

The South China Block was formed by collision at the end of the assembly of the Rodinia supercontinent (ca. 820 Ma; Li et al. 2009; Charvet 2013) and comprises the Yangtze Craton in the west and the Cathaysia Block in the east (Fig. 1a), which are separated by the Qin-Hang suture (Fig. 1b). The Jiangnan Orogen is located between the Yangtze and Cathaysia blocks, composed of Neoproterozoic arc terranes, which have experienced syn-schistose deformation and low-grade, greenschist-facies metamorphism, culminating with the intrusion of Neoproterozoic granites (the Jiuling batholith; 819 Ma) (Li et al. 2003; Sun and Chen 2017).

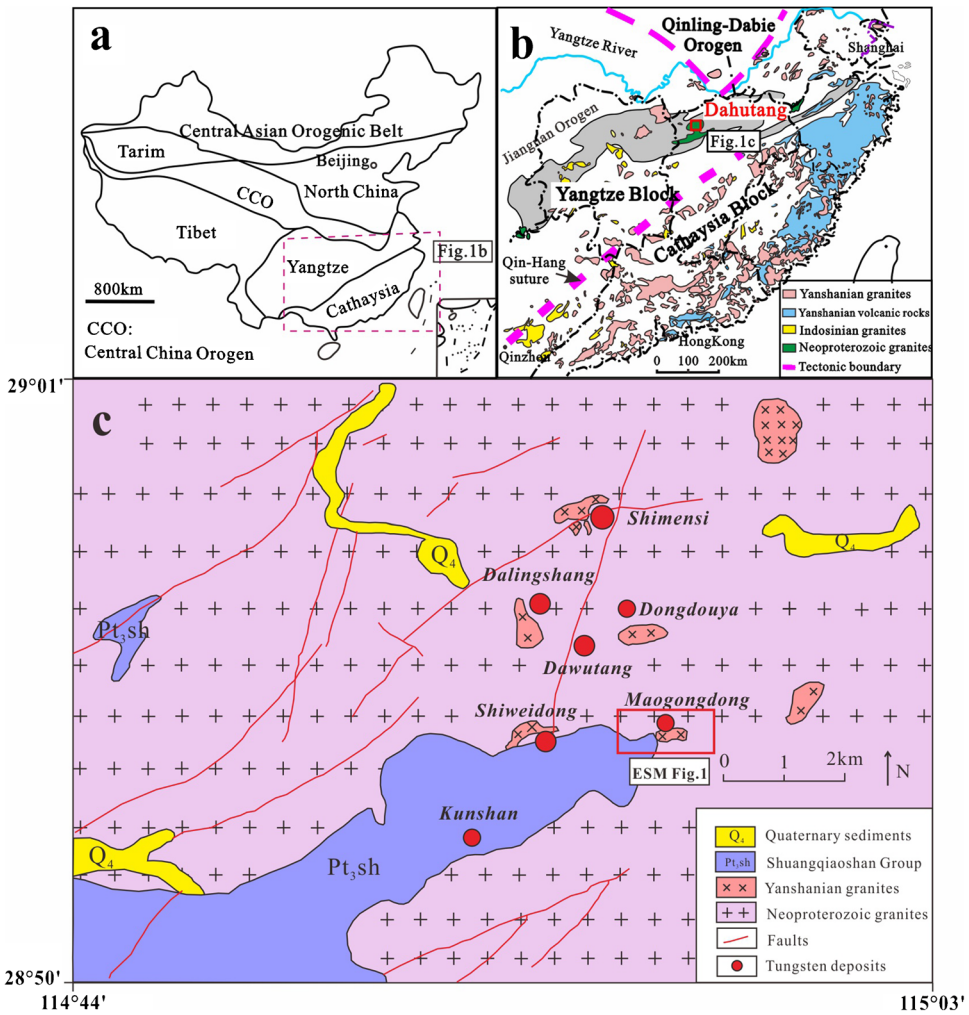


**Fig. 1** **a** Tectonic map of China showing the main tectonic units and the Yangtze and Cathaysia blocks in South China. **b** Distribution of granites and volcanic rocks in South China, showing the location of the Dahutang W-Cu-(Mo) ore field (modified after Zhou et al. 2006). **c** Geological map of the Dahutang ore field. The main ore deposits from north to south include Shimensi, Dalingshang, Dongdouya, Dawutang, Maogongdong, Shiweidong, and Kunshan (modified after Xiang et al. 2013; Jiang et al. 2015; Peng et al. 2018)

The Dahutang W-Cu-(Mo) ore field is located on the northern margin of the Jiangnan Orogen (Fig. 1a), consisting, from north to south, of the Shimensi, Dalingshang, Dongdouya, Dawutang, Shiweidong, and Kunshan deposits, and the newly discovered Maogongdong deposit (Fig. 1b, c) (Jiang et al. 2015; Peng et al. 2018). The exposed strata of the Dahutang district include the Neoproterozoic Shuangqiaoshan Group meta-sedimentary rocks (ca. 824 ± 5 Ma; Gao et al. 2012) (Fig. 1b), which are mainly composed of siltstone, tuffaceous sandstone, shale, and phyllite slate intercalated with minor pyroclastic volcanic rocks (BGMRJX 1984). Intrusive rocks in the Dahutang district consist of Neoproterozoic granodiorite and various Mesozoic (Yanshanian) granites (ca.150 to 130 Ma; Jiang et al. 2015; Song et al. 2018b). The Neoproterozoic Shuangqiaoshan Group and biotite granodiorite were intruded by Late Mesozoic granites, which mainly comprise porphyritic two-mica (biotite) granite, muscovite granite, and granite porphyry (Huang and Jiang 2014; Jiang et al. 2015). The Neoproterozoic granodiorite is part of the Jiuling batholith, which is the largest granitoid complex in southeastern China with an outcrop area of > 2300 $km^2$ (Xiang et al. 2013). The Neoproterozoic granodiorite and all phases of Mesozoic granites are documented as silica-rich, strongly peraluminous, exhibiting typical features of S-type granite (Huang and Jiang 2014; Wei et al. 2018). Integrated geochemical and Sr–Nd-Hf isotope studies show an anatectic sedimentary origin for these granitoids (Huang and Jiang 2014; Mao et al. 2015). The main geological structures of the Dahutang district include a series of EW- to NEE-, NE- to NNE-, NW-, and SW-trending faults (Fig. 1c).

The Maogongdong deposit has an established reserve of 11-kt $WO_3$ (average grade of 0.18%) in various types of W mineralization: vein-type, altered granite-type and greisen-type, among which the first type is of greatest importance, hosting > 95% of the total tungsten resource. The orebodies are mainly distributed in the east–west direction, occurring in the Neoproterozoic biotite granodiorites or in the contact between the Yanshanian muscovite granite and the Shuangqiaoshan Group strata (ESM Fig. 1).

## Mineral paragenesis of the Maogongdong deposit

According to the macroscopic and microscopic observation of mineral paragenesis and ore textural relationships, the mineralization process of the Maogongdong deposit can mainly be divided into four stages: (I) pre-ore stage, (II) tungsten mineralization stage, (III) sulfide stage, and (IV) post-ore stage (Fig. 2).

In the pre-ore stage (I) (ESM Fig. 2a – h), the main minerals are pure quartz veins (Qz1) that crosscut the granite (ESM Fig. 2h, i). Disseminated wolframite (Wol-1) (ESM Fig. 2b), scheelite (Sch-1) (ESM Fig. 2g), and sulfides occur occasionally in the altered granite affected by sericite alteration (ESM Fig. 2a).

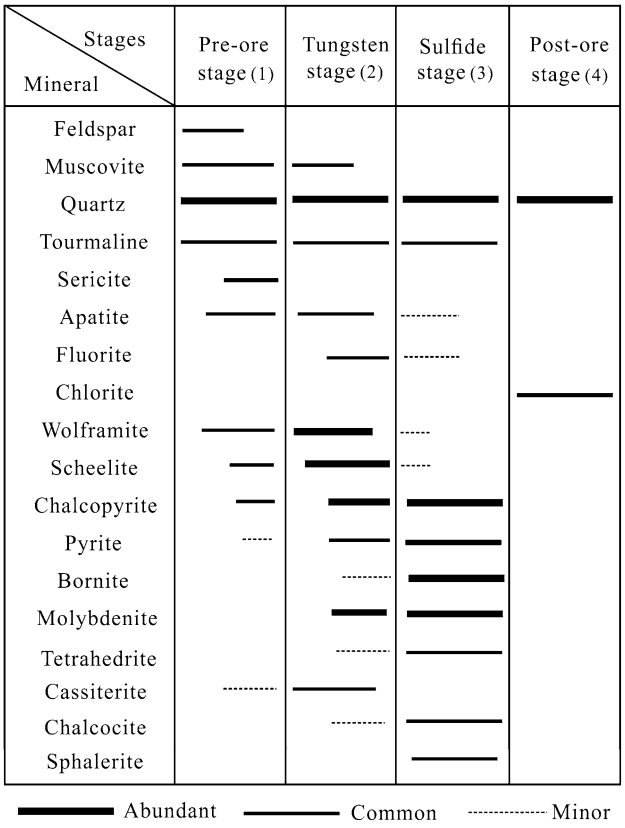


**Fig. 2** Paragenetic sequence diagram for mineral assemblages in the Maogongdong deposit

In the tungsten mineralization stage (II), the main ore minerals are wolframite ([Fe,Mn]$WO_4$) and scheelite ($CaWO_4$), mainly occurring in quartz veins (ESM Fig. 3a – r). Based on the petrographic characteristics, stage II can be further divided into two substages: early tungsten mineralization stage (II-a) and late tungsten mineralization stage (II-b), with the latter one being the main tungsten mineralization stage. In the stage II-a, the mineralization is relatively weak, with sparse disseminated wolframite (Wol-2a) and scheelite (Sch-2a) (1–5 vol%) in the early quartz veins (Qz-2a) (ESM Fig. 3a, b, c). In the stage II-b, the mineralization is greatly enhanced with dense disseminated, massive or granular wolframite (Wol-2b) and scheelite (Sch-2b and Sch-2c) (5–30 vol%) in the late quartz veins (Qz-2b) (ESM Fig. 3d – n).

Wolframite occurs as (1) fine-grained quartz–scheelite–wolframite in veinlets that crosscut muscovite granite (ESM Fig. 3a – d); (2) plate-like wolframite in greisen zones in the contact between quartz veins and the Shuangqiaoshan Group metasedimentary rocks (ESM Fig. 3e, f); (3) massive wolframite–scheelite–chalcopyrite–molybdenite–quartz ore (ESM

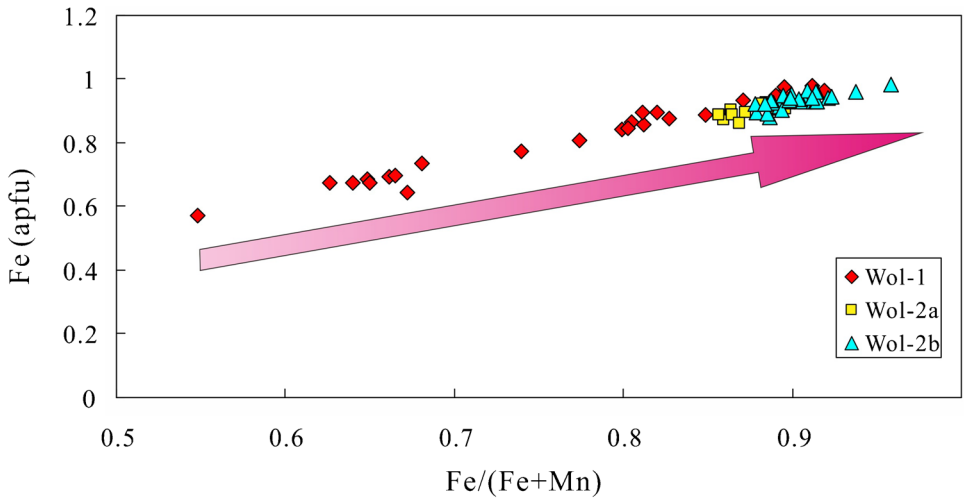


**Fig. 3** Plot of Fe/(Fe + Mg) in wolframite from the Maogongdong deposit

Fig. 3g); (4) wolframite–scheelite–fluorite–quartz veins in the Neoproterozoic granodiorite (ESM Fig. 3h, i).

Scheelite shows two types: (1) anhedral scheelite (Sch-2b) associated with dense disseminated wolframite (ESM Fig. 3j) and (2) subhedral scheelite (Sch-2c) in the interstitial space of quartz veins (ESM Fig. 3k-m). Scheelite occurs in the center of quartz veins, disseminated along the contact between quartz veins and the metasedimentary rocks, and within the strata (ESM Fig. 3n). Green fluorite also partly occurs within the Shuangqiaoshan Group strata (ESM Fig. 3o).

Under the microscope, silver-white wolframite crystals are generally replaced by scheelite–sulfide–quartz veinlets (ESM Fig. 3p – r). Some wolframite crystals are largely replaced by scheelite (ESM Fig. 3p). The scheelite veinlets that crosscut the wolframite crystals (ESM Fig. 3p) are replaced by later chalcopyrite (ESM Fig. 3p, q, r).

In the sulfide stage (III), mineral assemblage consists of mainly chalcopyrite and bornite, minor molybdenite, and little pyrite, tetrahedrite, chalcocite, and sphalerite. Acicular tourmaline is rare and occurs with minor wolframite, scheelite, molybdenite and fluorite in the quartz veins (Qz-3) (ESM Fig. 4a – h). Chalcopyrite always shows an intergrowth with subhedral pyrite (ESM Fig. 4a, b), with a clear and straight grain contact (ESM Fig. 4b). Sphalerite occurs as inclusions in chalcopyrite (ESM Fig. 4b). Some chalcopyrite is intergrown with molybdenite (ESM Fig. 4c), or replaced by bornite and covellite along grain margins (ESM Fig. 4d). Bornite is locally abundant and generally exhibits colorful features

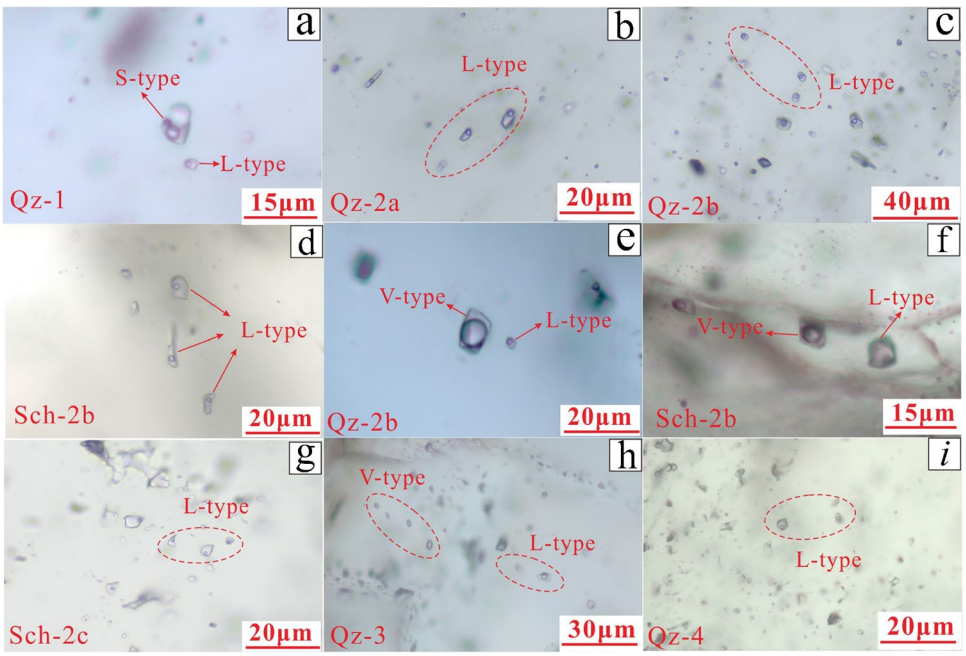


**Fig. 4** Photomicrographs of fluid inclusion assemblages (FIA) in transparent minerals of the Maogongdong deposit. **a** S-type inclusions in quartz of stage I. **b**, **c** L-type FIA in quartz of stage II-a and stage II-b. **d** L-type FIA in anhedral scheelite of stage II-b. **e**, **f** Coexistence of L-type and V-type inclusions in the same FIA with similar homogenization temperatures in quartz and anhedral scheelite of stage II-b. **g** L-type FIA in subhedral scheelite of stage II-b. **h** V-type FIA and L-type FIA in quartz of stage III. **i** L-type FIA in quartz of stage IV

and hexagonal crystal shape with a diameter of 5–30 mm (ESM Fig. 4e), intergrown with chalcopyrite and chalcocite (ESM Fig. 4f).

The post-ore stage (IV) is characterized by the formation of low-temperature alteration minerals, mainly chlorite, along with green quartz (Qz-4). These minerals surround the early white quartz–sulfide veins (Qz-3) as fillings of fractures at vein margins (ESM Fig. 4i).

## Samples and analytical methods

### EPMA analysis of major elements in wolframite

Wolframite was selected from 15 samples and analyzed by Electron Probe Micro Analyzer (EPMA). Five wolframite samples are from the altered muscovite granite (Wol-1), two from the early tungsten–quartz–vein stage, and eight from the late tungsten–quartz vein stage.

Mineral compositions of wolframite were determined at the State Key Laboratory of Geological Processes and Mineral Resources (SKL-GPMR), China University of Geosciences (Wuhan), with a JEOL JXA-8100 EPMA equipped with four wavelength-dispersive spectrometers (WDS). An accelerating voltage of 15 kV, a beam current of 20 nA, and a 2.5-μm spot size were used during the analysis. Data were corrected on-line using a ZAF (atomic number, absorption, fluorescence) correction procedure. The peak counting time was 10 s for Na, Mg, Al, Si, K, Ca, Fe, F, Ta, Nb, Pb, Zn, Sn, W and 20 s for Mn and Ti, and the corresponding detection limits (wt%) are 0.02% (Na, K, Ca, Mg, Al. Mn), 0.03% (Fe, Ti), 0.04% (Nb, Sn), 0.05% (Si, Pb, W), 0.07% (Zn), 0.12% (Ta), and 0.18% (F). The contents of Na, Al, Si, K, F, Ta, Pb, Zn, and Sn in most wolframite samples are below the detection limit. The background counting time was set to one-half of the peak counting time on the high- and low-energy background positions.

### Fluid inclusion measurements

Representative samples of wolframite, scheelite, fluorite, and quartz in different mineralization stages of the Maogongdong deposit were chosen for fluid inclusion study. In the pre-ore stage, a total of 21 fluid inclusion assemblages (FIAs) in quartz were selected for fluid inclusion microthermometry study. In the early tungsten stage, 16 FIAs in wolframite and 17 FIAs in quartz were analyzed. In the late tungsten mineralization stage, 42 FIAs in wolframite, 36 FIAs in scheelite, 16 FIAs in fluorite, and 59 FIAs in quartz were measured. In the sulfide stage, a total of 48 FIAs in quartz were measured. In the post-ore stage, a total of 18 FIAs were measured in quartz from quartz–chlorite veins.

Fluid inclusions in wolframite were observed using an Olympus BX51 infrared microscope equipped with a high-resolution IR (Infrared) camera in the fluid inclusion laboratory at Collaborative Innovation Center for Exploration of Strategic Mineral Resources, China University of Geosciences, Wuhan, and the microthermometric measurements for scheelite, fluorite, and quartz were taken using a Linkam THMSG600 heating/freezing stage mounted on a Leica DM 2500P microscope in the same laboratory. Heating and cooling rates were 20–30 °C/min and less than 1 °C/min when close to phase transitions. The precision of the measurements is ± 0.2 °C from − 196 to 0 °C and ± 1 °C from 100 to 600 °C. The last ice-melting temperature (Tm) was used for salinity estimation (Bodnar 1993).

The composition of single inclusions was measured with a Renishaw RM-1000 Laser Raman spectrometer at the SKL-GPMR, China University of Geosciences, Wuhan. An Ar + (532.5 nm) laser with a source power of 20 mW (2 mW power on sample surface) was used.

### Hydrogen, oxygen, and carbon isotope analysis

Selected minerals from quartz veins in the Maogongdong deposit were prepared and observed under the microscope. Representative samples were chosen for picking mineral separates for oxygen, hydrogen, and carbon isotope analysis, including 7 wolframite samples and 13 quartz samples. The minerals were handpicked under a binocular microscope. Finally, 20 oxygen isotope data (7 of wolframite, 13 of quartz), 17 hydrogen isotope data (5 of wolframite, 12 of quartz), and 13 carbon isotope data (3 of wolframite, 10 of quartz) were obtained.

The H-O-C isotopic compositions were analyzed using a Finnigan MAT253 mass spectrometer in the Laboratory of Stable Isotope Geochemistry, Institute of Mineral Resources, Chinese Academy of Geological Sciences in Beijing. Oxygen isotope analyses for quartz and wolframite were performed by the conventional $BrF_5$ method described by Clayton and Mayeda (1963). Hydrogen and carbon isotopic analysis of fluid inclusions of minerals includes the following main steps: pre-treatment by vacuum devaporizing at 150 °C for more than 4 h, in order to completely remove surface adsorbed water and secondary inclusion water. Then, the samples were heated up to 400–500 °C to release $H_2O$ from the fluid inclusions and reacted with zinc to produce $H_2$. The carbonaceous material in mineral fluid inclusions is extracted by thermal decrepitation and separated simultaneously during the hydrogen isotope analysis. The material was subsequently oxidized to $CO_2$ using CuO at 800 °C for isotope analysis. The δD and $\delta^{18}O$ data are reported relative to the

V-SMOW standard, with the analytical error of ± 2 ‰ for δD and ± 0.2 ‰ for $\delta^{18}O$. The analytical accuracy of $\delta^{13}C$ is ± 0.2 ‰, and the data are reported relative to V-PDB.

#### Sulfur isotope analysis

In situ LA-MC-ICP-MS sulfur isotope analysis was conducted on selected sulfides from 16 samples in the pre-ore stage, tungsten mineralization stage, and sulfide stage. A total of 153 points were collected. Laser sampling was performed by a Resonetics-S155 excimer ArF laser ablation system, and sulfur isotope ratios were analyzed with a Nu Plasma II MC-ICP-MS at SKL-GPMR. All analyses were made using a 33-μm laser beam with a repetition rate of 8 Hz, an ablation time of 40 s, and an energy of 3 J/cm$^2$.

The national pyrite standard WS-1 was used in this study. The standard-sample-standard bracketing method was applied to measure the $\delta^{34}S$ values. The $\delta^{34}S_{VCDT}$ values (1.1 ± 0.2 ‰) of WS-1 were determined with SIMS at the Chinese Academy of Geochemistry, Guangzhou (Zhu et al. 2016). The international reference standard sphalerite NBS-123 ($\delta^{34}S_{VCDT}$ = + 17.1 ‰) and also the WS-1 standard were used to calibrate the mass bias for sulfur isotopes, to avoid matrix effects (Zhu et al. 2016). The true sulfur isotope ratio is calculated by correcting the instrumental mass bias by linear interpolation between the biases calculated from two neighboring standard analyses. Isotope ratio data are reported relative to Vienna Cañon Diablo troilite (V-CDT) in terms of conventional per mil deviation (‰). The analytical uncertainties in this study are about 0.1 ‰. Detailed analytical conditions and procedures can be seen in Zhu et al. (2017).

## Results

### Chemical composition of wolframite

The results for major element compositions of wolframite analyzed by EPMA are summarized in ESM Table 1 and illustrated in Fig. 3. The wolframite Wol-1 (pre-ore stage) has a major element composition different from Wol-2a and Wol-2b (tungsten stage), displaying lower FeO contents (13.6–23.0 wt%), higher MnO contents (1.98–11.1 wt%), and similar $WO_3$ contents (72.2–76.0 wt%). The Wol-2a (early tungsten stage) exhibits relatively higher FeO (20.3–22.1 wt%) and lower MnO (2.44–3.49 wt%), and 75.9–76.9 wt% $WO_3$. The Wol-2b (late tungsten stage) displays the highest FeO (20.8–23.3 wt%) and lowest MnO (0.99–2.99 wt%), and 73.8–77.1 wt% $WO_3$. The Fe/(Fe + Mn) of Wol-1, Wol-2a, Wol-2b wolframite show an increasing trend from 0.55–0.92, to 0.86–0.90, and 0.88–0.96.

## Fluid inclusions

### Petrography and types of fluid inclusions

Representative samples of wolframite (Wol-2a, Wol-2b), scheelite (Sch-2b, Sch-2c), fluorite (Fl), and quartz (Qz-1, Qz-2, Qz-3, Qz-4) were selected for fluid inclusion study.

The genetic classification of fluid inclusions was conducted in accordance with the following criteria: randomly isolated fluid inclusions and clustered fluid inclusions in intragranular position were considered as primary in origin, whereas those aligned along microfractures in transgranular trails were designated secondary (Roedder 1984; Lu et al. 2004; Ni et al. 2015a, b). In order to avoid misinterpretation, secondary FIs were not documented in this study. Detailed fluid inclusion petrography at room temperature (25 °C) revealed three types: (1) liquid-rich two-phase (L-type), (2) vapor-rich two-phase (V-type), (3) three-phase aqueous inclusions containing black solid crystal(s) (S-type).

L-type inclusions are always the most abundant at all stages, accounting for more than 95% of the total inclusion numbers. They contain a vapor phase occupying 5–40 vol% of the inclusion volume, with the diameter of 3–40 μm and mainly ellipsoidal and irregular in shape (Figs. 4 and 5). V-type inclusions predominantly occur in quartz at the sulfide stage, partially visible in minerals at the tungsten mineralization stage, representing about 4% of the total numbers. They are generally round or irregular in shape and 5–30 μm in diameter, with 50–80 vol% vapor bubbles (Figs. 4e, f, h and 5f). S-type inclusions are scarce (less than 1%), with daughter minerals almost insoluble and small, and can only be observed in the quartz of stage I (Fig. 4a). They are mainly ellipsoidal or irregular in shape, and 4 to 12 μm in size, with their vapor bubbles occupying less than 30 vol%.

#### Laser Raman spectroscopic results

Laser Raman spectroscopic analyses indicate that the liquid phases of primary inclusions are almost pure $H_2O$, whereas the vapor phases are dominated by $H_2O$ and some $CH_4$, followed by $N_2$, with trace $CO_2$ and $H_2S$. Fluid inclusions in quartz of the pre-ore stage mainly contain $CH_4$ besides $H_2O$; some of them contain a small amount of $N_2$ (ESM Fig. 5a). In the tungsten mineralization stage, $CH_4$ and $N_2$ are well developed in the vapor phase (both V type and L type fluid inclusions), all found in quartz coexisting with disseminated wolframite (ESM Fig. 5b), quartz coexisting with massive wolframite and scheelite (ESM Fig. 5c), and scheelite (ESM Fig. 5d, e). In the sulfide stage, fluid inclusions contain rare but significant $CO_2$ and $H_2S$ besides $CH_4$ and $N_2$ (ESM Fig. 5f).

**Table 1** Summary of microthermometric data on fluid inclusions of the Maogongdong deposit

| Stage | Host Mineral | Type | FIs Type | FIA Number | Th(°C) | | | Peak range of Th(°C) | Tm(°C) | | | Salinity (wt.%NaCl.eq) | | |
|---|---|---|---|---|---|---|---|---|---|---|---|---|---|---|
| | | | | | Max | Min | Avg | | Max | Min | Avg | Max | Min | Avg |
| Pre-ore stage (1) | Quartz | Qz-1 | L | 19 | 422 | 381 | 401 | 390 – 410 | -1.5 | -3.3 | -2.4 | 6.4 | 2.8 | 4.6 |
| | | | L + S | 2 | 416 | 406 | 411 | | -2.0 | -2.3 | -2.2 | 5.3 | 3.7 | 4.5 |
| Tungsten stage (2) | Wolframite | Wol-2a | L | 16 | 384 | 352 | 369 | 360 – 380 | -1.9 | -3.3 | -2.7 | 6.4 | 3.4 | 5.0 |
| | Quartz | Qz-2a | L | 17 | 324 | 369 | 348 | 330 – 360 | -1.2 | -3.4 | -2.3 | 6.6 | 2.2 | 4.3 |
| | Wolframite | Wol-2b | L | 37 | 366 | 314 | 341 | 325 – 355 | -2.1 | -3.9 | -2.8 | 7.6 | 3.9 | 5.3 |
| | | | L + V | 5 | 361 | 343 | 350 | | -2.1 | -2.6 | -2.4 | 4.9 | 3.9 | 4.5 |
| | Scheelite | Sch-2b | L | 20 | 343 | 295 | 318 | 310 – 330 | -1.2 | -3.7 | -2.5 | 7.2 | 2.2 | 4.8 |
| | | | L + V | 3 | 346 | 298 | 321 | | -2.1 | -2.5 | -2.3 | 4.7 | 3.8 | 4.3 |
| | Quartz | Qz-2b | L | 54 | 338 | 271 | 303 | 280 – 320 | -1.4 | -3.8 | -2.5 | 7.4 | 2.6 | 4.7 |
| | | | L + V | 5 | 319 | 307 | 315 | | -2.0 | -2.9 | -2.3 | 5.5 | 3.6 | 4.3 |
| | Scheelite | Sch-2c | L | 13 | 299 | 273 | 285 | 275 – 295 | -2.0 | -2.9 | -2.6 | 5.6 | 3.6 | 4.8 |
| | Fluorite | Fl | L | 16 | 298 | 263 | 283 | 270 – 290 | -1.1 | -2.8 | -2.0 | 5.3 | 1.9 | 3.7 |
| Sulfide stage (3) | Quartz | Qz-3 | L | 33 | 223 | 288 | 254 | 240 – 270 | -1.4 | -3.3 | -2.3 | 6.4 | 2.6 | 4.3 |
| | | | L + V | 10 | 241 | 278 | 258 | | -2.0 | -2.8 | -2.3 | 5.2 | 3.7 | 4.4 |
| | | | V | 5 | 244 | 264 | 256 | | -1.4 | -2.5 | -2.0 | 4.6 | 2.6 | 3.8 |
| Post-ore stage (4) | Quartz | Qz-4 | L | 18 | 157 | 206 | 183 | 160 – 190 | -1.0 | -2.2 | -1.5 | 4.1 | 1.8 | 2.8 |

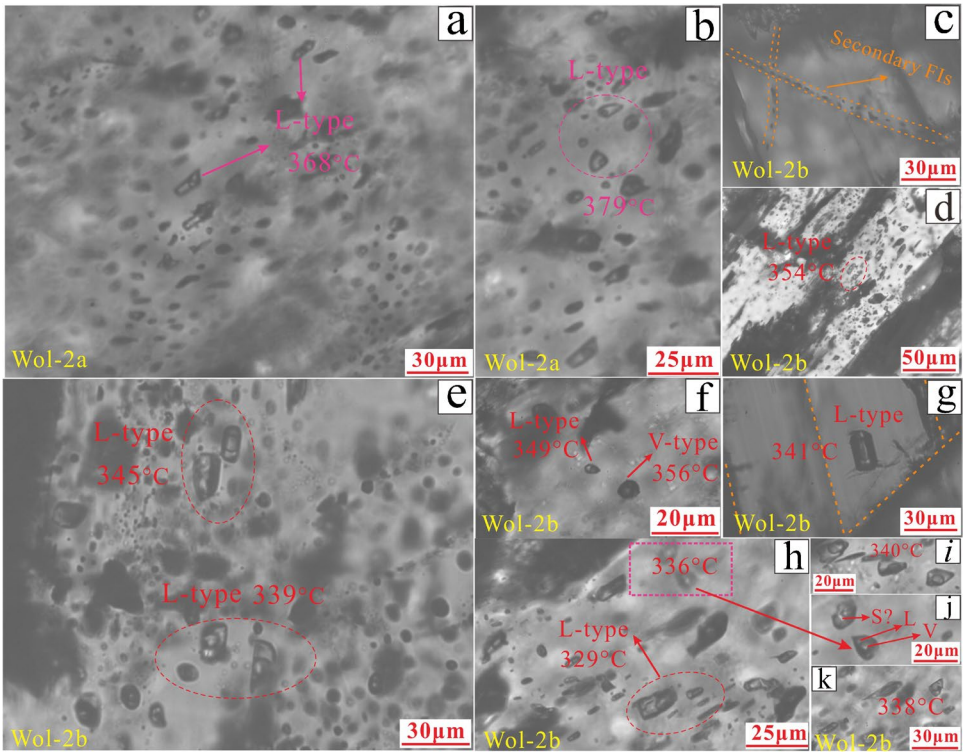


**Fig. 5** Photomicrographs of fluid inclusions assemblages (FIA) in wolframite of the Maogongdong deposit. **a**, **b** L-type FIA in wolframite of the early tungsten mineralization stage (stage II-a). **c** Secondary FIA in wolframite of the late tungsten mineralization stage (stage II-b). **d** L-type FIA in plate-like wolframite along with greisenization. **e** L-type FIA in massive wolframite ore. **f** Coexistence of L-type and V-type inclusions in the same FIA with similar homogenization temperature. **g** Isolated inclusions in wolframite. **h**, **i**, **j**, **k** L-type FIA in wolframite of quartz–scheelite–wolframite veins of the late tungsten mineralization stage

### Microthermometry of fluid inclusions

Microthermometric measurements of fluid inclusions in wolframite were conducted on FIAs (Goldstein and Reynolds 1994; Chi and Lu 2008). A single FIA represents temporally coeval inclusions mainly present in clusters. We selected FIAs showing the least evidence of necking-down or shape modifications for further microthermometric measurements. The microthermometric data are reported as average of two-to-five primary inclusions with similar shape in each FIA, and the final results are summarized in Table 1 and illustrated in Figs. 6 and 7.

In the pre-ore stage (I), FIAs in quartz veinlets (Qz-1) mostly consist of L-type (about 98 %), and very few S-type (about 2 %) (Fig. 4a). A total of 21 FIAs were selected for fluid inclusion microthermometric study. The homogenization temperatures of FIAs in quartz range from 381 to 422°C (peak at 390−410°C, average 402°C), while the ice-melting temperatures and corresponding salinities are −3.3 to −1.5°C (average −2.4°C) and 2.8 to 6.4 wt% NaCl equiv. (average 4.6 wt%).

In the early tungsten mineralization stage (II-a), fluid inclusions are mainly L-type. There are 16 FIAs in wolframite (Wol-2a) and 17 FIAs in quartz (Qz-2a) analyzed. In wolframite, infrared microthermometric data show that FIAs have ice-melting temperatures from − 3.3 to − 1.9 °C (average − 2.7 °C), equivalent to salinities of 3.4 − 6.4 wt% NaCl equiv. (average 5.0 wt%), and homogenization temperatures of 352 − 384 °C (peak at 360 − 380 °C, average 369 °C). In quartz, the homogenization temperatures range from 324 to 369 °C (peak at 330 − 360 °C, average 348 °C) and the ice-melting temperatures range from − 3.4 to − 1.2 °C (average − 2.3 °C), indicating salinities of 2.2 − 6.6 wt% NaCl equiv. (average 4.3 wt%).

In the late tungsten mineralization stage (II-b), a total of 153 FIAs have been measured in wolframite (Wol-2b), disseminated scheelite (Sch-2b), subhedral scheelite (Sch-2c), fluorite (Fl), and quartz (Qz-2b). Most FIAs are characterized by a dominance of L-type inclusions (Figs. 4c-g and 5), whereas some FIAs are characterized by coexisting L-type and V-type, typically shown in wolframite (Fig. 5f), disseminated scheelite (Fig. 4f), and quartz (Fig. 4e). The microthermometric measurements of FIAs show significantly different homogenization temperatures among these different minerals (Figs. 6, 7). Different kinds of wolframite in stage II-b exhibit similar microthermometric results. The infrared microthermometric study shows that homogenization temperatures of FIAs in wolframite have a range of 314 to 366 °C (peak at 325 − 355 °C, average 341 °C), and ice-melting temperatures vary from − 3.9 to − 2.1 °C, equivalent to salinities from 3.9 to 7.6 wt% NaCl equiv. In disseminated scheelite (Sch-2b) intergrown with wolframite, the homogenization temperatures of FIAs are different from wolframite, ranging from 295 to 346 °C (peak at 310–330 °C, average 319 °C). However, their ice-melting temperatures are similar, varying from –3.7 to –1.2 °C (average –2.5 °C),

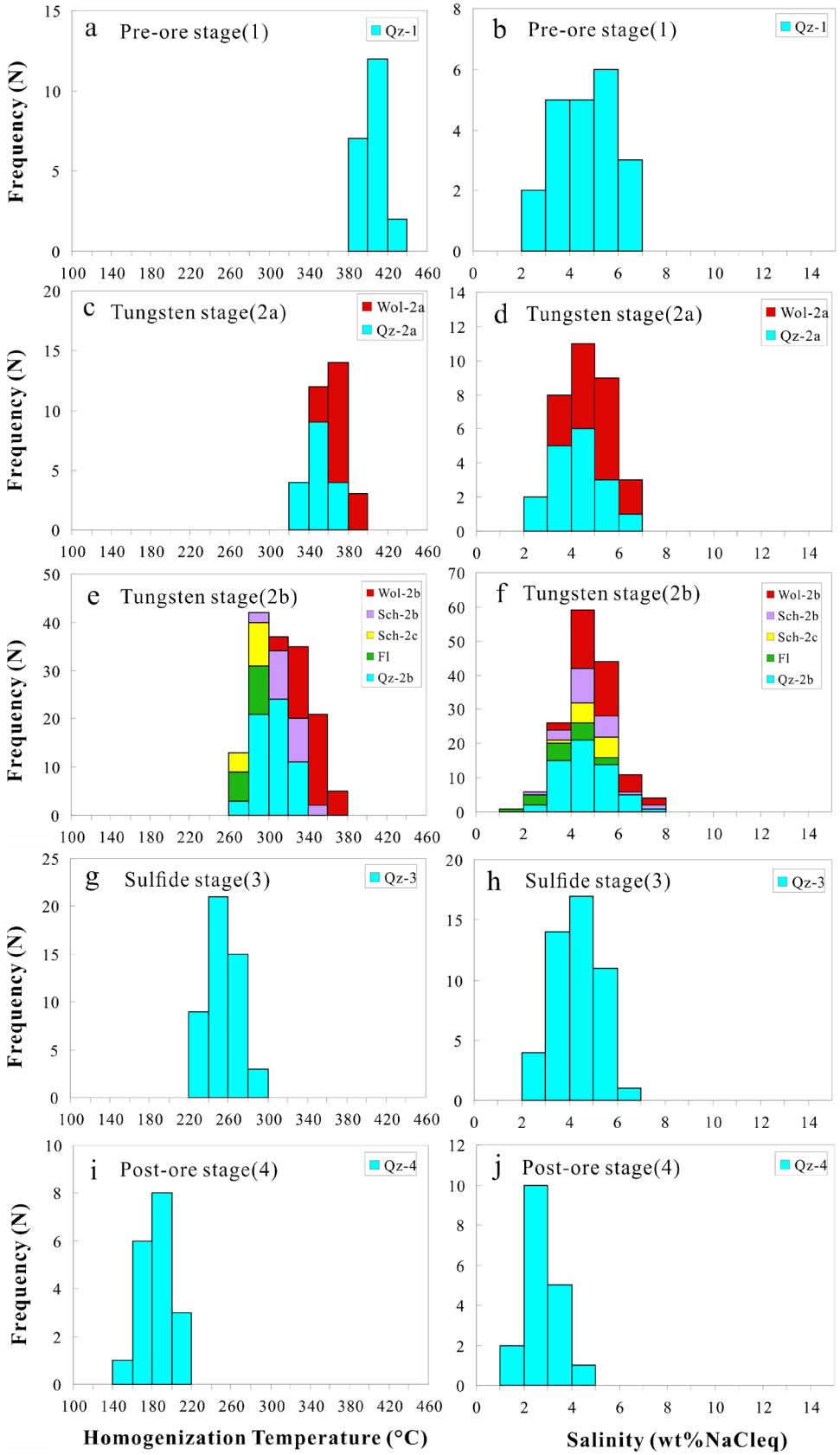


**Fig. 6** Histograms of homogenization temperatures (left) and salinities (right) of fluid inclusions from different ore stages and host minerals in the Maogongdong deposit

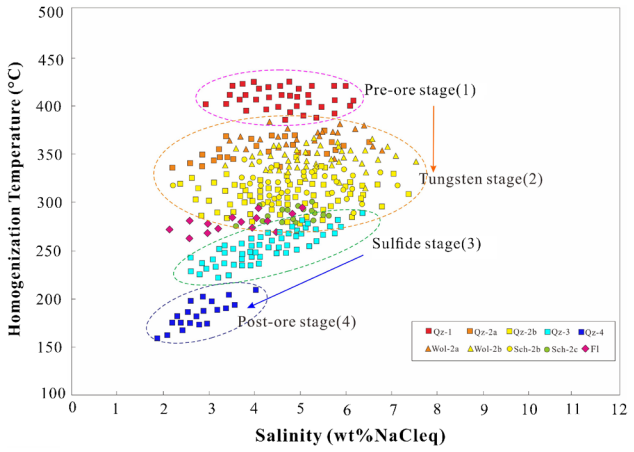


**Fig. 7** Homogenization temperature versus salinity of fluid inclusion assemblages from different ore stages in the Maogongdong deposit

corresponding to salinities of 2.2 to 7.2 wt% NaCl equiv. (average 4.7 wt%). In the quartz (Qz-2b), the homogenization temperatures of FIAs show a lower and relatively broad range from 271 to 338 °C (peak at 280–320 °C, average 304 °C), while the ice-melting temperatures and corresponding salinities are –3.8 to –1.4 °C (average –2.5 °C) and 2.6 to 7.4 wt% NaCl equiv. (average 4.6 wt%). The homogenization temperatures of FIAs in the subhedral scheelite (Sch-2c) and fluorite (Fl) are lowest among numerous minerals in stage II-b, displaying a range of 273 to 299 °C (peak at 275–295 °C, average 285 °C) in subhedral scheelite and 263 to 298 °C (peak at 270–290 °C, average 283 °C) in fluorite. The ice-melting temperatures and corresponding salinities of subhedral scheelite are similar to other minerals, with –2.9 to –2.0 °C (average –2.6 °C) and 3.6 to 5.6 wt% NaCl equiv. (average 4.8 wt%), but slightly lower in fluorite, exhibiting a range of –2.8 to –1.1 °C (average –2.0 °C) and 1.9 to 5.3 wt% NaCl equiv. (average 3.7 wt%). For the minerals in this stage (Wol-2b, Sch-2b, Qz-2b), the coexistence of L-type and V-type in the same FIA is occasionally but characteristically observed, which yield similar homogenization temperatures and slightly lower salinities of V-type than L-type inclusions, suggesting local fluid boiling in stage II-b.

In the sulfide stage (III), in addition to common L-type inclusions, V-type inclusions are also developed. Many FIAs are characterized by V-type or coexistence of L-type, V-type inclusions (Fig. 5h), besides L-type inclusions. A total of 48 FIAs were measured in this stage. The homogenization temperatures of L-type, L + V type, V-type FIAs, respectively, range from 223 to 288 °C, 241 to 278 °C, 244 to 266 °C, and the ice-melting temperatures, respectively, range from –3.3 to –1.4 °C, –2.8 to –2.0 °C, –2.5 to –1.4 °C, indicating corresponding salinities of 2.6–6.4, 3.7–5.2, 2.6–4.6 wt% NaCl equiv.. In the same FIAs, the coexisting L-type and V-type inclusions commonly yield similar homogenization temperatures, and the L-type inclusions have salinities slightly higher than the V-type inclusions, indicating fluid immiscibility in stage III.

In the post-ore stage (IV), fluid inclusions are mostly of L-type (Fig. 5i) and slightly less in number and smaller in size, compared with the sulfide stage. A total of 18 L-type FIAs were measured in quartz from the post-ore stage quartz–chlorite veins (Qz-4). The homogenization and ice-melting temperatures of FIAs are remarkably lower than those in the sulfide stage. The homogenization temperatures range from 157 to 206 °C (peak at 160–190 °C, average 183 °C) (Fig. 6i), and the ice-melting temperatures are –2.2 to –1.0 °C (average –1.5 °C), corresponding to salinities of 1.8 to 4.1 wt% NaCl equiv. (average 2.8 wt%).

## H-O-C-S isotopes

### Hydrogen and oxygen isotope data

The analytical results on H–O isotopes of selected minerals (quartz and wolframite) from different ore stages from the Maogongdong deposit are listed in ESM Table 2 and illustrated in Fig. 8. The δD values measured by fluid inclusions range from − 91 to − 63 ‰. There is little difference in the δD value of fluid in quartz in each stage, which is − 64 ‰ (n = 1) (stage II-a), − 78 to − 65 ‰ (n = 7, average − 71 ‰) (stage II-b), − 73 to − 63 ‰ (n = 3, average − 68 ‰) (stage III) and − 65 ‰ (n = 1) (stage IV). Compared with the δD values in coexisting quartz, the δD values of fluid in wolframite are greatly reduced, ranging from − 91 to − 75 ‰ (n = 5, average − 85 ‰) (stage II-b).

The $\delta^{18}O$ values of fluids in equilibrium with quartz were calculated using the quartz–water equation of Clayton et al. (1972), and fluids in equilibrium with wolframite were calculated using the quartz–wolframite equation of Zhang et al. (1994). These calculations yielded $\delta^{18}O_{fluid}$ values of 1.6 to 7.5 ‰, with a $\delta^{18}O_{fluid}$ value 7.5 ‰ in the early tungsten mineralization stage, 5.3 to 6.9 ‰ in the late tungsten mineralization stage (n = 8, average 6.0 ‰), 3.9 to 4.3 ‰ in the sulfide stage (n = 3, average 4.1 ‰), and 1.6 ‰ in the post-ore stage. Compared with quartz (12.7 to 14.0 ‰), the $\delta^{18}O$ values of wolframite are lower (2.8 to 6.4 ‰; n = 7, average 4.2 ‰), and the corresponding $\delta^{18}O_{fluid}$ value of wolframite (4.1 to 7.5 ‰) is similar to that calculated for quartz (5.3 to 6.9 ‰).

### Carbon isotope data

The C isotope compositions were measured by fluid inclusions in quartz and wolframite selected from different ore stages, ranging from − 26.2 to − 11.9 ‰ (ESM Table 2; Fig. 9). In the early tungsten mineralization stage (II-a), $\delta^{13}C$ values of quartz coexisting with sparse disseminated

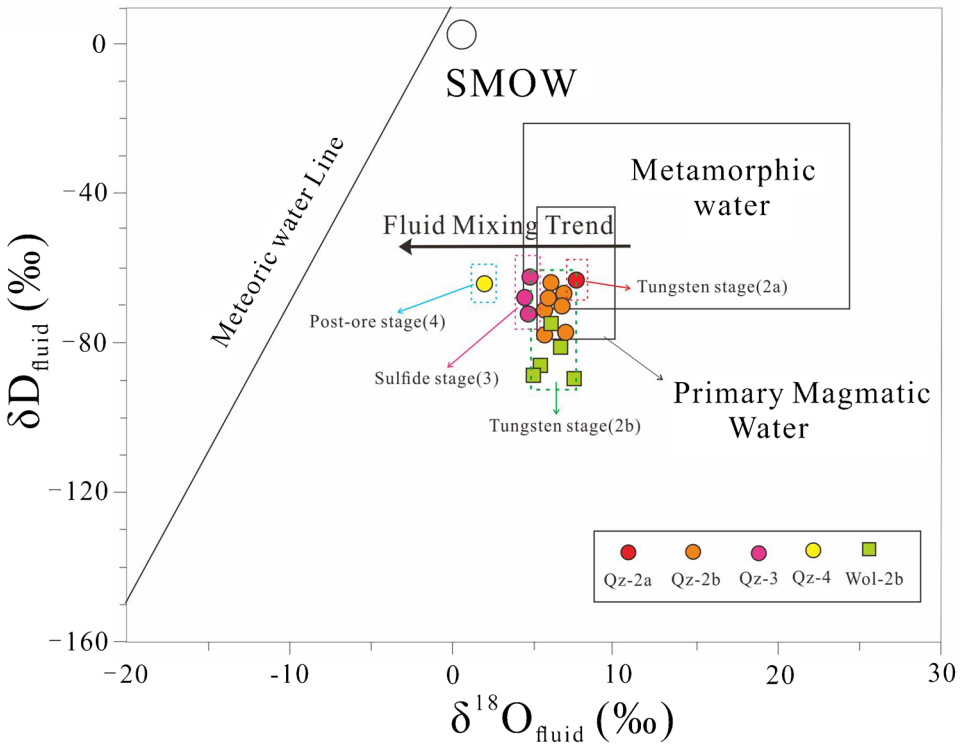


**Fig. 8** Calculated oxygen and hydrogen isotopic compositions of fluids in equilibrium with different ore stages and minerals from the Maogongdong deposit

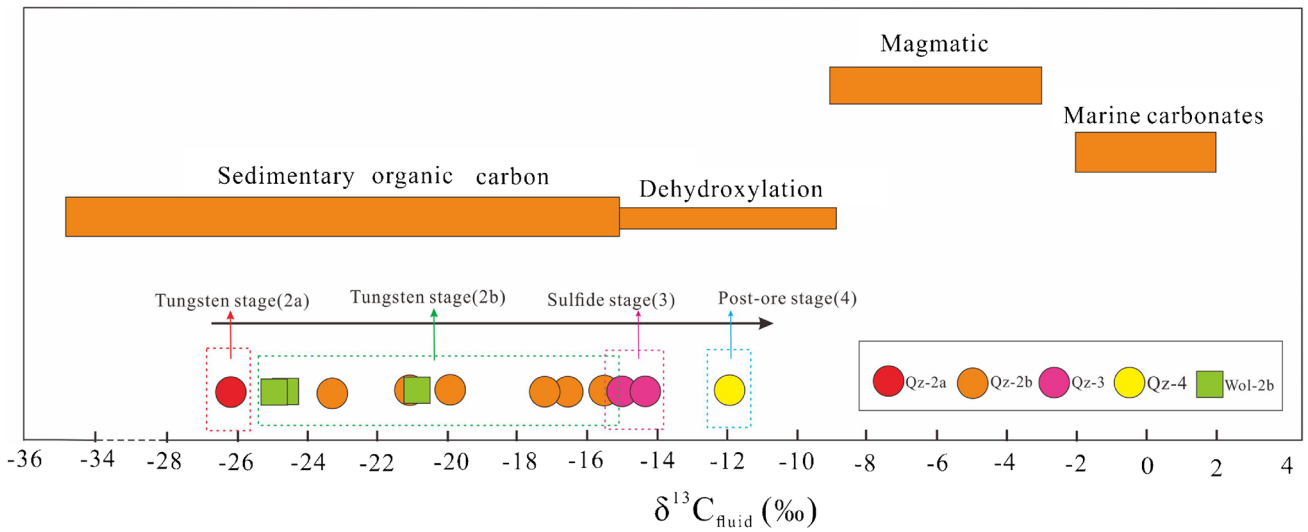


**Fig. 9** Carbon isotopic compositions of fluids in different ore stages from the Maogongdong deposit

wolframite show the lowest value (−26.2 ‰), and in the main tungsten mineralization stage (II-b), the $\delta^{13}C$ values increase slightly, with wolframite at −25.2 to −21.0 ‰ (n = 3, average −23.6 ‰) and quartz at −23.5 to −15.5 ‰ (n = 6, average −19.1 ‰). In the sulfide stage (III), the carbon isotopic composition is further increased, with −15.1 to −14.5 ‰ (n = 2, average −14.8 ‰), and in the final post-ore stage (IV), the $\delta^{13}C$ value is the least negative (−11.9 ‰).

### Sulfur isotope data

The S isotopic compositions are shown in ESM Table 3 and Fig. 10. A total of 16 samples, 153 points in three stages were collected for in situ sulfur isotope analysis. In the pre-ore stage (I), the $\delta^{34}S$ values range from −1.7 to 0.6 ‰ for sulfides in muscovite granite (n = 25; average −0.6 ‰), including pyrite from −0.8 to 0.6 ‰ (n = 8; average −0.1 ‰) and chalcopyrite from −1.7 to −0.9 ‰ (n = 17;

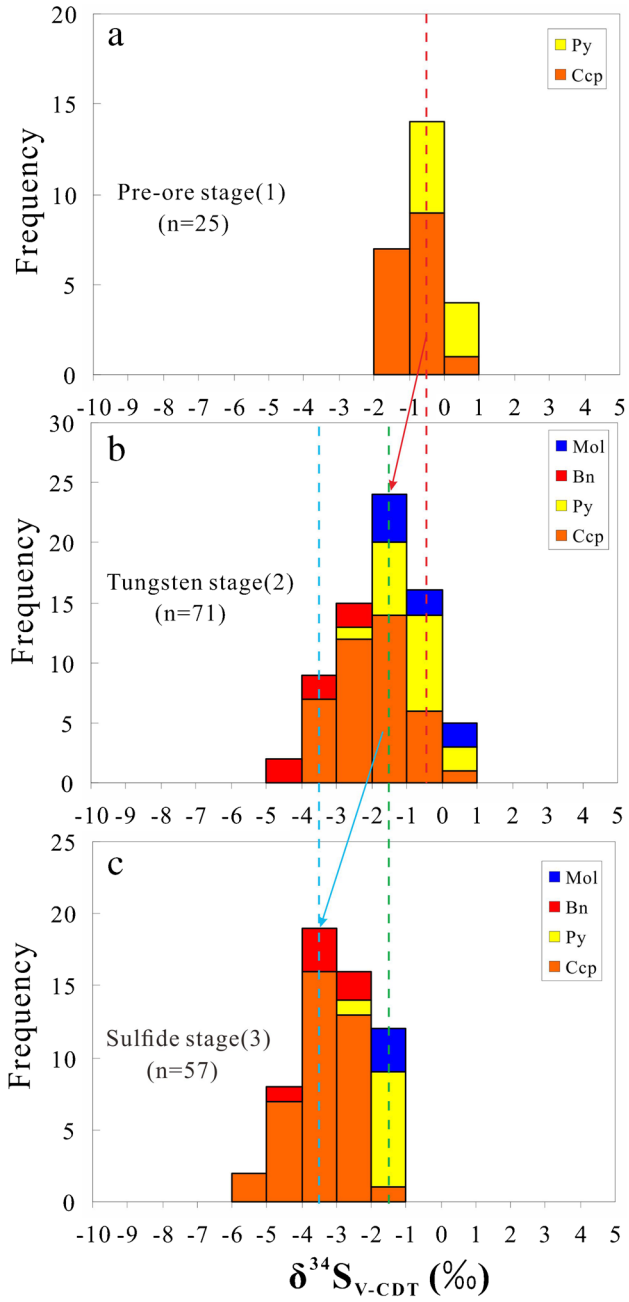


**Fig. 10** Histogram of sulfur isotopic compositions of sulfide minerals in different ore stages from the Maogongdong deposit

average – 0.9 ‰). Compared to magmatic sulfur, the $\delta^{34}S$ values in the tungsten mineralization stage (II) are slightly lower, ranging from – 4.5 to 0.7 ‰ (n = 71; average – 1.7 ‰), with pyrite from – 2.4 to 0.5 ‰ (n = 17; average – 0.9 ‰), bornite from – 4.5 to – 2.3 ‰ (n = 6; average – 3.6 ‰), molybdenite from – 1.6 to 0.7 ‰ (n = 8; average – 0.9 ‰), chalcopyrite from – 3.7 to 0.1 ‰ (n = 40; average – 2.0 ‰). The $\delta^{34}S$ values are further reduced in the sulfide stage (III), ranging from – 5.2 to – 1.3 ‰ (n = 57; average – 3.0 ‰), with pyrite from – 2.2 to – 1.6 ‰ (n = 9; average – 1.8 ‰), bornite from – 4.5 to – 2.5 ‰ (n = 6; average – 3.4 ‰), molybdenite from – 1.7 to – 1.3 ‰ (n = 3; average – 1.4 ‰), chalcopyrite from – 5.2 to – 1.5 ‰ (n = 39; average – 3.4 ‰).

## Discussion

### Sources and P-T-S-ρ evolution of ore-forming fluids

The $\delta D_{fluid}$-$\delta^{18}O_{fluid}$ diagram (Fig. 8) and ESM Table 2 indicate that the fluid in the early tungsten mineralization stage (II-a) is within the range of magmatic water (Ohmoto 1986). In tungsten deposits of the Dahutang ore field, meteoric water is usually added in the late ore stage, as observed in the Dalingshang deposit (Peng et al. 2018) and Shimensi deposit (Song et al. 2018a). As shown in Fig. 8, the Maogongdong H–O isotopes also show an evolution trend toward meteoric water, which is not particularly obvious but visible in the late tungsten mineralization stage (II-b), while further exceeding the range of magmatic water in the sulfide stage (III), and deviating completely in the late post-ore stage (IV), implying increasing mixing with meteoric water during the hydrothermal evolution. As in the model put forward by Zhou et al. (2001), the percentage of meteoric water can be approximately estimated by the difference between the initial fluid and fluid in each stage. For the Maogongdong deposit, the amount of meteoric water is 2.5 – 12.5% in stage II-b, about 20% in stage III and 35 – 40% in stage IV, respectively. Thus, we conclude that the ore-forming fluids of the Maogongdong deposit were initially derived from magmatic fluids exsolved during the magmatic–hydrothermal transition and then diluted by meteoric water in the evolving hydrothermal system. The wolframite samples show lower δD values than primary magmatic water (Fig. 8), which may be due to early degassing in the open magma system, resulting in a generally low δD value of $CH_4$ and $H_2O$ in the wolframite fluid inclusions (Taylor 1986; Shmulovich et al. 1999).

The petrographic and microthermometric measurement of fluid inclusions suggests that the physicochemical properties of the fluids were variable during the different ore-forming stages in the Maogongdong deposit. As a whole, there is the trend of progressively decreasing temperature from early to late stage, while salinities are almost unchanged in stage I to II but slightly decreased in stage III to IV (Figs. 6, 7). The evolution of the fluids is discussed in detail below.

In the pre-ore stage (I), the pristine ore-forming fluid of the Maogongdong deposit originates from magmatic water and belongs to a high-temperature, moderate- to low-salinity, low-density and low-oxygen-fugacity NaCl-$H_2O$-($CH_4$-$N_2$) system, which is different from skarn tungsten deposits, which are characterized by high salinity in the early ore

stage (Meinert et al. 2005; Bodnar et al. 2014; Jiang et al. 2020). The fluid inclusions in pure quartz veinlets (Qz-1) are characterized by L-type FIAs and insoluble daughter-minerals. The black insoluble daughter minerals are also found in other deposits in the Dahutang ore field, such as the Dalingshang deposit (Peng et al. 2018), and consist mainly of sulfides (i.e., chalcopyrite), which indicates that the hydrothermal fluids had inherited considerable amounts of ore metals when they exsolved from the residual melts. The homogenization temperatures and salinities of fluid inclusions allow estimate the density and pressure of the ore-forming fluids (Fig. 11; Bischoff et al. 1991; Bodnar 1993; Bodnar and Vityk 1994). For the fluid of the pre-ore stage, a density of 0.48 – 0.62 g/cm$^3$ is estimated (Fig. 11a) and a lithostatic pressure in the range of 260 – 360 MPa (mainly 285 – 320 MPa) (Fig. 11b), corresponding to a depth of 9.6 – 13.3 km (mainly 10.6 – 11.9 km) (rock density of 2.7 g/cm$^3$).

The characteristics of the ore-forming fluid in the early tungsten mineralization stage (II-a) are similar to that in the pre-ore stage. In the late tungsten mineralization stage (II-b), the temperature of the ore-forming fluid significantly decreased and there are obvious differences in fluid inclusions between different minerals. For the dominant minerals in this stage (Wol-2b, Sch-2b, Qz-2b), occasionally but characteristically the coexistence of L-type and V-type can

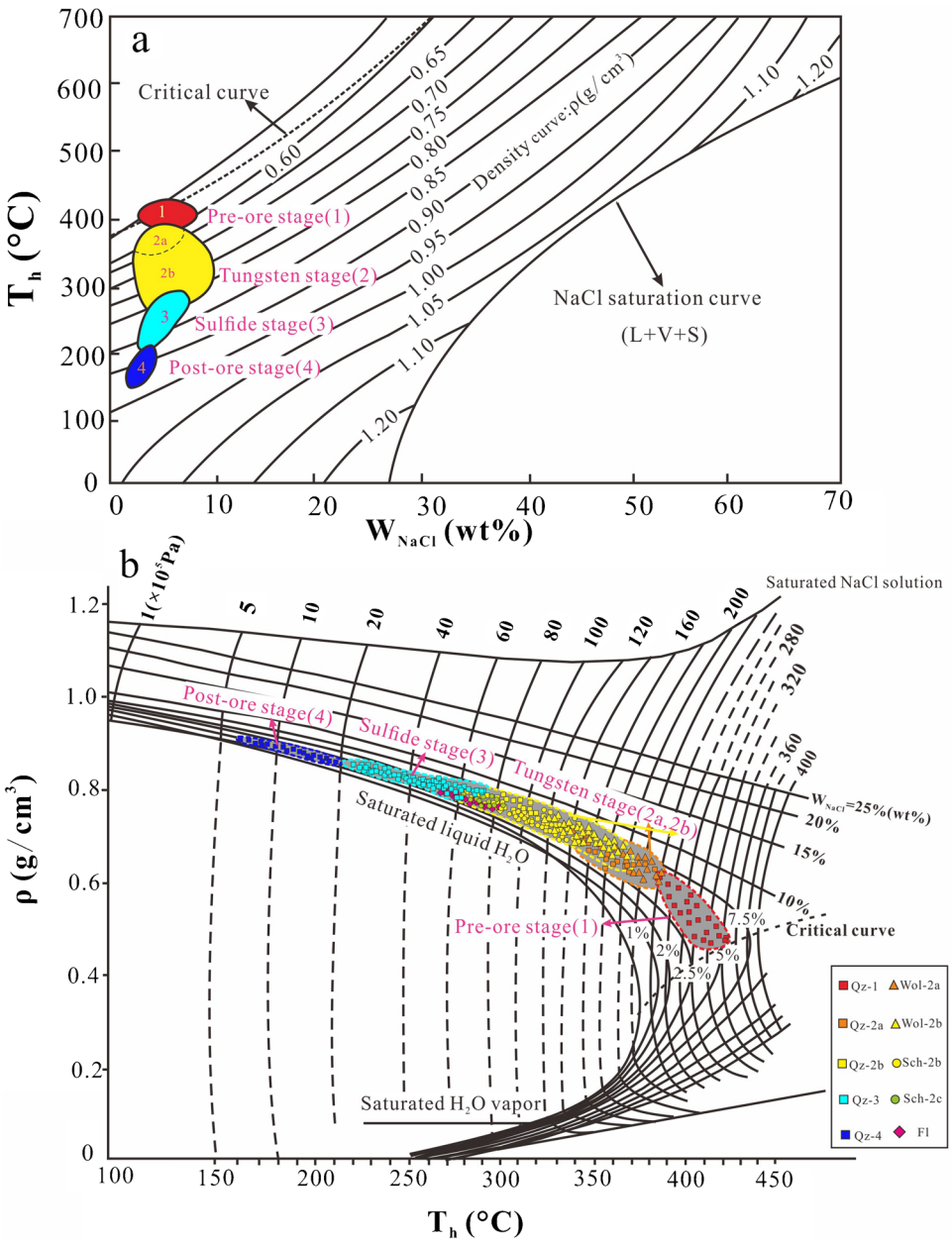


**Fig. 11** **a** Density estimations of fluid in different ore stages of the Maogongdong deposit, **b** pressure estimations of fluid in different ore stages of the Maogongdong deposit (after Bischoff et al. 1991; Bodnar 1993; Bodnar and Vityk 1994)

be observed in the same FIA, which yielded similar homogenization temperatures and slightly lower salinities of V-type than L-type inclusions, suggesting local fluid boiling in the late tungsten mineralization stage (Lu et al. 2004; Xiong et al. 2017; Ni et al. 2015a, b). For the fluid of the early tungsten mineralization stage (II-a), the density of 0.58 – 0.71 g/cm$^3$ is estimated, and lithostatic pressure with the range of 140 – 260 MPa (mainly 180 to 240 MPa) (Fig. 11), equivalent to a depth of 5.2 – 9.6 km (mainly 6.7–8.9 km). For the fluid of the late tungsten mineralization stage (II-b), the density of 0.66 – 0.82 g/cm$^3$ is estimated and lithostatic pressure with the range of 50 – 220 MPa (mainly 75 to 150 MPa) (Fig. 11), equivalent to a depth of 1.9 – 8.1 km (mainly 2.8–5.6 km).

In the sulfide stage (III), the homogenization temperatures of FIAs further decrease. In the same FIAs, the coexisting L-type and V-type inclusions commonly show similar homogenization temperatures, and the L-type inclusions have salinities slightly higher than in the V-type inclusions, indicating fluid immiscibility in stage III. For the fluid of this stage, the density of 0.79 – 0.88 g/cm$^3$ is estimated and lithostatic pressure of 20 to 75 MPa (mainly 30 to 60 MPa) (Fig. 11), corresponding to a depth of 0.7 to 2.8 km (mainly 1.1 to 2.2 km).

Based on microthermometric data, Song et al. (2018a) used the Flincor program to suggest that the depth for the greisenization and major mineralization at Dahutang ore field likely was no deeper than 7.8 km, while the polymetallic sulfide mineralization occurred no deeper than 6.1 km. In this study, the estimated depth of the tungsten mineralization stage is 1.9 – 8.1 km (mainly 2.8–5.6 km), and the estimated depth of the sulfide stage is 0.7 to 2.8 km (mainly 1.1 to 2.2 km), which is similar to but more precise than the previous studies.

In the post-ore stage (IV), the fluids are characterized by the mixing of magmatic water with meteoric water with high density, low temperature, and low salinity. The formation temperature and fluid salinity are the lowest, and the density is estimated to be 0.87 – 0.93 g/cm$^3$, with a lithostatic pressure of 6 to 20 MPa (mainly 8 to 16 MPa) (Fig. 11), corresponding to a lithostatic depth of 0.2 to 0.7 km (mainly 0.3 to 0.6 km).

## Comparison of fluid inclusions in ore and gangue minerals

Previous studies show that there can be great differences of petrography and microthermometric result of fluid inclusions between coexisting ore and gangue minerals, especially the homogenization temperature of fluid inclusions can be higher in the ore mineral compared to the gangue mineral by up to 100 °C (Campbell 1990; Cao et al. 2009; Ni et al. 2015a, b; Chen et al. 2018). It is generally considered that the beginning precipitation of ore minerals is earlier than gangue minerals (Ni et al. 2015a, b; Chen et al. 2018); hence, it is necessary to accurately measure the homogenization temperatures of FIs in ore and gangue minerals in order to reflect the true mineralization process.

The petrography and microthermometric results of fluid inclusions in the ore and gangue minerals in the Maogongdong deposit also exhibit various characteristics, indicating that they would not form simultaneously (ESM Fig. 2 and Table 1). In the early tungsten mineralization stage (II-a), the homogenization temperature of fluid inclusions in wolframite is about 25 °C higher than that of quartz in the same vein. In the late tungsten mineralization stage (II-b), the homogenization temperature of fluid inclusions in wolframite is about 20 °C higher than that of anhedral scheelite and generally 40 °C higher than that in adjacent quartz. It is also about 60 °C higher than that of subhedral scheelite and fluorite. These results indicate that wolframite likely crystallized earlier than the coexisting scheelite and quartz, which is also supported by the textural relationship where wolframite commonly is crosscut by scheelite–quartz veinlets or occurs in the center of the veins and is partly replaced by scheelite (ESM Fig. 3p).

## Source and significance of carbon

Carbon isotope is often used to indicate the source of ore-forming materials in ore deposits (Faure 1986; Ohmoto 1986; Hoefs 1997). In general, there are three major carbon sources: a marine carbonate source with a $\delta^{13}C$ mean value of 0 ‰ (Ohmoto 1986); a mantle source with a $\delta^{13}C$ mean value of – 5 ‰ (Hoefs 1997); and an organic matter source with a $\delta^{13}C$ mean value of – 25 ‰ (Faure 1986). There is relatively little published data on carbon isotopes from the Dahutang ore field. Based on the $\delta^{13}C$ values of the calcite in the late ore stage, such as – 12.3 and – 10.2 ‰ in the Kunshan deposit (Zhang et al. 2018) and – 11.4 to – 5.7 ‰ in the Shimensi deposit (Ruan et al. 2015), it is suggested that carbon was initially from a magmatic source and subsequently mixed with organic carbon. In this way, it is limited to ensure the source of mixed carbon in the late ore stage, but lacks the direct carbon isotope features in the main ore stage.

In this study, the carbon isotopes were measured by fluid inclusions of minerals in different ore stages in order to clarify the source and variation of carbon. Our new data (Fig. 9) show that the carbon in the ore-forming system exhibits obvious characteristics of sedimentary organic carbon at the early hydrothermal ore stage (– 26.2 to – 21.0 ‰), which is much lower than the magmatic carbon source (– 7 to – 3 ‰; Hoefs 1997). Therefore, it is suggested that sedimentary carbon was not added in the late stage but already added in the magmatic fluid system before hydrothermal mineralization. The surrounding Shuangqiaoshan Group

meta-sedimentary rocks can provide sufficient organic carbon (BGMRJX 1984; Gao 2012). Considering the addition of organic carbon, there are two possibilities: one is the melt that might assimilate organic matter during its ascent and emplacement and then organic matter decomposed to $CH_4$, $N_2$, $H_2O$ under such high temperature and pressure, and another possibility is the assimilation of carbon from the host strata during the magmatic–hydrothermal transition stage, resulting in obvious organic carbon characteristics in the early ore-forming fluid. In the latter case, it is difficult to imagine that such low $\delta^{13}C$ values can be obtained in almost all minerals. Meanwhile, it is also unable to account for the low $\delta^{13}C$ values of fluid inclusions in quartz vein occurred in the Yanshanian granites, which were not directly contacted with the Shuangqiaoshan Group. Therefore, we favor the scenario where the carbon signature was acquired during magmatic stage by assimilation of rocks from the Shuangqiaoshan Group. This is consistent with some previous studies in the Dahutang ore field; for example, it is concluded that the causative Yanshanian S-type granites in the Dahutang ore field are product of partial melting from Shuangqiaoshan Group rocks (Jiang et al. 2015; Fan et al. 2019), and the oxygen fugacity of granites is relatively low as deduced by mineralogical work such as mica and zircon (Huang and Jiang 2014; Zhang et al. 2019). The addition of organic carbon from the Shuangqiaoshan Group yields relatively reduced conditions, which are beneficial for bivalent Fe transport, and this facilitates the deposition of wolframite. At the same time, in a reduced environment, sulfur prefers to occur as negative bivalent sulfur, contributing to subsequent copper–molybdenum mineralization. In the late ore stage, the escape of volatile $CH_4$ characterized with low $\delta^{13}C$ values leads to the gradual increase in carbon isotope value in the fluid.

## Sulfur isotope characteristics and indicative geothermometer

The various values of sulfur isotopes in different ore-forming stages and minerals are shown in ESM Table 3 and Fig. 10. The sulfides from the pre-ore stage show quite uniform $\delta^{34}S$ values (− 1.7 to 0.6 ‰), which is consistent with previously published data of the Shimensi deposit ($\delta^{34}S = -3.1$ to 1.0 ‰; Xiang et al. 2013). A narrow range of $\delta^{34}S$ values with a mean close to zero indicates a possible magmatic source for sulfur (Ohmoto 1972). However, $\delta^{34}S$ values of sulfides from the pre-ore stage to the tungsten mineralization stage show a decreasing trend (Fig. 10), reducing to a range of − 4.5 to 0.7 ‰, and this tendency is more obvious to the later sulfide stage, displaying $\delta^{34}S$ values from − 5.2 to − 1.3 ‰. This variation of sulfur isotopic composition within and between mineral grains indicates that biogenic sulfur may not play an important role during sulfide precipitation (Peng et al. 2018). Instead, this variation may be the result of the changes in $fO_2$ and pH as the fluids evolved (Rajabpour et al. 2017). Based on the S-C isotope model of Ohmoto (1972), we consider that the depleted sulfur isotope values are likely generated by an increase of oxygen fugacity due to the inflow of oxidized meteoric waters (as evidenced from H–O isotopes), which is also indicated by the first appearance of $CO_2$ (from $CH_4 \rightarrow CO_2$) in fluid inclusions measurement in the sulfide stage.

In the sulfide stage, sulfides show variable $\delta^{34}S$ values (ESM Table 3 and Fig. 10). The comparison of sulfur isotope values ($\delta^{34}S_{Mol} > \delta^{34}S_{Py} > \delta^{34}S_{Ccp} > \delta^{34}S_{Bn}$) indicates that the ore minerals basically reach the sulfur isotope equilibrium during precipitation (Ohmoto 1986; Rollinson 1993). Equilibrium between sulfide phases can also be derived from petrographic features such as the closely coexisting chalcopyrite and pyrite with clear and straight boundaries, and subhedral mineral grains (ESM Fig. 4b). According to the formula: $\delta^{34}S_{(Py\text{-}Ccp)} = 4.5 \times 10^5/T(°K)^2$ (Kajiwara and Krouse 1971), four pairs of $\delta^{34}S$ values measured from coexisting chalcopyrite and pyrite (ESM Fig. 6) were selected to calculate equilibrium temperature of sulfur isotopes. Sulfur isotope thermometer displays equilibrium temperature of 242 to 290 °C, showing that the precipitation temperature of copper ore is similar to but a little higher than the homogenization temperature of fluid inclusions in quartz (223 − 288 °C), which may be due to the early formation of sulfide.

## The role of fluid–rock reaction during mineralization

Fluid–rock reaction plays an important role in the formation of many tungsten deposits (Jiang et al. 2020; Mao et al. 2020). On the one hand, water–rock reaction can directly provide ore-forming materials, such as Ca, Fe, Mn, Mg, and S; on the other hand, when the fluid interacts with the surrounding rocks, the temperature, pH and $fO_2$ of the hydrothermal solution will change and lead to a change in the solubility of the ion complex, then resulting in the precipitation of ore minerals.

In many Sn-W deposits, greisenization and chloritization are often regarded as a favorable sign of mineralization (Pirajno 2009). Tin mineralization occurs in the alteration zone close to the intrusive rock body, while the W in the same mineralization system often forms later and migrates farther with the fluid and precipitates in the vein system far away from the intrusive rock body. Therefore, it is believed that the surrounding rock alteration represented by greisenization has a significant impact on the precipitation of tin (Schmidt et al. 2020). For the formation of skarn W deposit, it is generally recognized that the influence of fluid–rock reaction is crucial (Kwak 1987; Meinert 2005). However, it has been controversial whether

fluid–rock reaction plays an important role in the formation of vein-type W deposits. Most researchers focused on fluid mixing, boiling, and cooling, only some believe that fluid–rock reaction is also an important reason for changing fluid properties and causing tungsten mineral precipitation (Guillemette and Williams-Jones 1993; Macey and Harris 2006; Lecumberri-Sanchez et al. 2017; Sun and Chen 2017; Peng et al. 2018; Jiang et al. 2020).

The contact zone between the Dahutang Mesozoic granite and Neoproterozoic granodiorite and the Shuangqiaoshan Group surrounding rocks widely developed hydrothermal alteration such as greisenization, tourmalinization, silicification and chloritization, especially the greisenization is most intense and is closely related to veinlet-disseminated orebodies. In the Maogongdong deposit, it can be seen that a large amount of wolframite occurs in the greisenization contact zone between hydrothermal quartz veins and the Shuangqiaoshan Group strata, as well as the scheelite and fluorite in the quartz vein occurring within the Shuangqiaoshan Group (ESM Fig. 3e, f, n, o). This indicates that there may be a certain amount of Fe and Ca released from biotite and feldspar during the process of fluid–rock reaction. The reaction process could be expressed as follows:

$$K(Mg,Fe)_3AlSi_3O_{10}(F,OH)_2(biotite) + 2Al^{3+} \rightarrow KAl_2\left[AlSi_3O_{10}\right](OH)_2(muscovite) + 3Fe^{2+} \quad (1)$$

$$NaAlSi_3O_8CaAl_2Si_2O_8(plagioclase) + 2H^+ + K^+ \rightarrow KAl_2KAl_2\left[AlSi_3O_{10}\right](OH)_2(muscovite) + 2SiO_2(quartz) + Na^+ + Ca^{2+} \quad (2)$$

The Fe/(Fe + Mn) of hydrothermal wolframite is higher than that of wolframite in the muscovite granites, which can be explained by the addition of Fe (Fig. 3). Previous studies also confirm that fluid–rock reaction can provide ore-forming materials for tungsten-bearing hydrothermal fluids, such as the study of boron isotopes and Ca, Sr and V content variations in tourmaline (Hu and Jiang 2020) and the trace elements variations of scheelite in the Dahutang ore field (Peng et al. 2018). Therefore, the fluid–rock interaction may be an important factor for the genesis of the giant Dahutang tungsten deposits.

## Ore-forming process of the Maogongdong deposit

Based on petrographic evidence and geological analysis, the ore-forming process in the Maogongdong deposit can be mainly divided into a tungsten-dominated mineralization stage and a copper–molybdenum-dominated mineralization stage. On the whole, the tungsten ores generally formed earlier than the copper and molybdenum ores, and their geneses are related to magmatic–hydrothermal evolution.

### Main tungsten mineralization

Tungsten is a strongly incompatible lithophile element, with an abundance in the crust of more than 100 times higher than in the mantle (Liu et al. 1982). The Shuangqiaoshan Group in the Dahutang ore field is an important tungsten-bearing formation, generally with high tungsten content, such as mudstone contains an average of 9.13 ppm W, much higher than the average 1.0 ppm in crust (Rudnick and Gao 2004; Liu et al. 1982). Thus, it may be an important source of tungsten in this ore field (Jiang et al. 2015).

In the Maogongdong deposit, it is suggested that during the magmatic–hydrothermal transition stage, the ore-forming hydrothermal fluid differentiated from the magma, containing of W, Cu, Mo and other metal elements, and replaced the previous silicate minerals such as mica, feldspar, and tourmaline. This resulted in the small-scale altered granite-type tungsten ores, sericite and nodular tourmaline (Fig. 12a, b) (Hu and Jiang 2020). In the hydrothermal stage, the scale and type of ore mineralization are closely related to the temperature of the fluid and fluid–rock reaction. The initial high temperature magmatic fluid (390 − 410 °C) differentiated from the muscovite granite and then formed a relatively pure quartz veinlet (Qz-1). In the early tungsten mineralization stage (330 − 380 °C), fluid cooling led to the decrease in tungsten complex solubility and thus small-scale wolframite and scheelite precipitated (Fig. 12c). After that, the temperature and pressure of the ore-forming fluid kept decreasing in the late tungsten mineralization stage (280 − 355 °C), and a large amount of tungsten ore minerals crystallized, particularly with obvious greisenization at the contact zone of the surrounding rock (Fig. 12d, e, f). In this process, $WO_4^{2-}$ preferentially combines with high concentrations of $Fe^{2+}$ and $Mn^{2+}$ to form wolframite, followed by $Ca^{2+}$ to form scheelite. At the same time, fluid boiling in a small scale may also contribute to the crystallization of tungsten ores. After the wolframite (Wol-2b) and anhedral scheelite (Sch-2b) precipitated completely, the continuous addition of external Ca led to the crystallization of subhedral scheelite (Sch-2c) and fluorite (275 − 295 °C). In the late hydrothermal stage, when the temperature dropped to about 270 °C, most of the tungsten has precipitated, and the sulfide mineralization gradually developed.

### Copper–molybdenum mineralization

In addition to tungsten ores, there is also a large amount of copper in the Dahutang area, mainly occurs as chalcopyrite and bornite, and a small amount of tetrahedrite and chalcocite. Similar to the tungsten, the copper in the

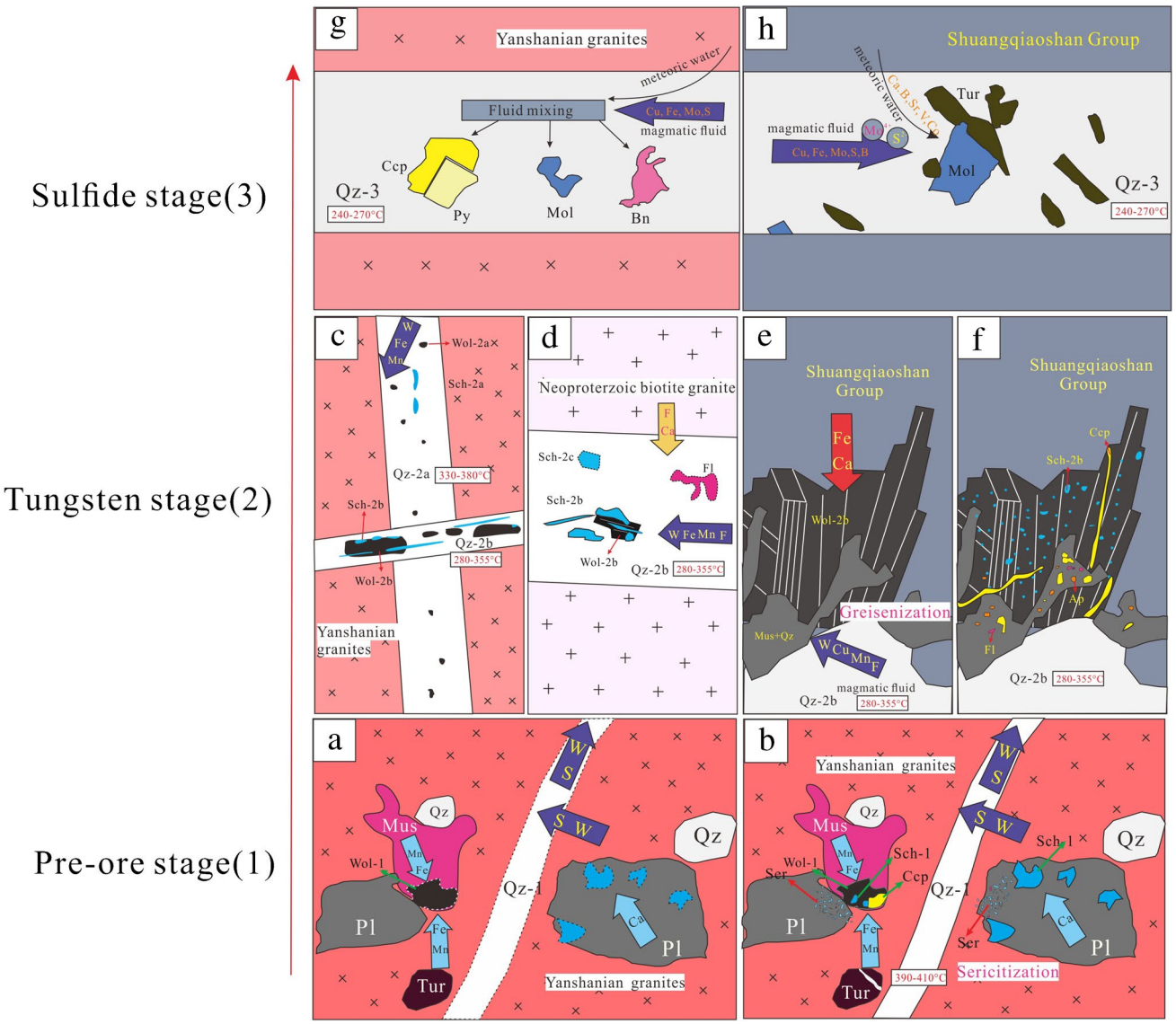


**Fig. 12** A sketch diagram illustrating ore-forming processes of the Maogongdong deposit

Maogongdong deposit may be derived from the Shuangqiaoshan Group, which is rich in copper (Jiang et. al 2015; Sun et al. 2018). Most of the copper minerals occur in hydrothermal quartz veins with medium–low formation temperature (240 – 270 °C), and a few are disseminated in granites. According to the results of S isotope data in different ore stages (Fig. 10), sulfur exhibits magmatic source. From the temperature salinity and the H–O isotope plots (Figs. 7, 8), it can be seen that much meteoric water was added in the sulfide stage. The mixing of the two different fluids changed the physical and chemical conditions of the ore-forming environment, leading to the crystallization of molybdenum and copper ores (Fig. 12g, h). This can also be evidenced from the characteristics of fluid inclusions in quartz in the sulfide stage, which is characterized by the appearance of $CO_2$ and $H_2S$ (ESM Fig. 5f).

## Conclusions

(1). The Maogongdong W–(Cu–Mo) deposit is mainly a vein-type deposit, characterized by early W and late Cu–Mo mineralization.

(2). Geological, petrography, fluid inclusions and H-O-S stable isotope data suggest that the Maogongdong deposit belongs to a high-to-moderate temperature, moderate-to-low salinity, and low-oxygen fugacity fluid system. The early ore-forming fluids are mainly

magmatic water with relatively high temperature (270–410 °C) and moderate-to-low salinity, while the late ore-forming fluids are a mixture of magmatic and meteoric water, with medium–low temperature (160–270 °C) and low salinity.

(3). Carbon isotope values show that a large amount of organic carbon from the Shuangqiaoshan Group country rocks was added before mineralization, which kept the whole system at low redox conditions.

(4). The greisenization is the result of the reaction between the ore-forming fluid and the surrounding rocks. In this process, a large amount of Fe and Ca were added to the ore-forming system.

(5). The fluid cooling and pressure decrease are the main factors causing tungsten ore crystallization, while local boiling may also make a contribution, and fluid–rock reaction provides the supplementary source of ore-forming materials.

## Author's information

The first author Da-Long Hu is a PhD candidate in the China University of Geosciences in Wuhan, who is working on tungsten mineralization in south China. The corresponding author Shao-Yong Jiang is a professor in Economic Geology and Geochemistry in the China University of Geosciences in Wuhan, who works on mineral deposit geochemistry.

**Supplementary Information** The online version contains supplementary material available at https://doi.org/10.1007/s00126-022-01114-2.

**Acknowledgements** We give special thanks to the 916 Geological Team and the Northwest Jiangxi Geological Team for their helpful assistance in field work. Sincere thanks are given to Drs. Dao-Hui Pi, Yao-Ming Xu, Ning-Jun Peng for their support in sample preparation and discussion. We are also grateful to Drs. Kui-Dong Zhao and Shui-Yuan Yang for their help with laboratory work. Chief Editor Prof. Bernd Lehmann and Associate Editor Prof. Ruizhong Hu and two reviewers provided valuable comments and suggestions, which improved this manuscript significantly. This work is supported by grants from the National Natural Science Foundation of China (No. 92162323) and the MOST Special Fund from the State Key Laboratory of Geological Processes and Mineral Resources, China University of Geosciences (No. MSFGPMR03-2).

**Authors' contributions** S.-Y. J. conceived the whole project; D.-L. H and S.-Y. J. conducted the field work and collected samples; D.-L. H performed the analytical work; S.-F.X., J.-X. D., and K.-X. W. involved in part of the analytical work; D.-L. H and S.-Y. J. wrote the manuscript; all authors contributed to revisions of the manuscript.

**Funding** This work is supported by funding from the National Natural Science Foundation of China (No. 92162323) and the MOST Special Fund from the State Key Laboratory of Geological Processes and Mineral Resources, China University of Geosciences (No. MSFGPMR03-2).

**Data Availability** All the data are included in this paper as electric supplementary materials and can be downloaded from the journal website or contact the authors for data requests。

## Declarations

**Ethics approval and consent to participate** Not applicable.

**Consent for publication** Not applicable.

**Competing interests** All authors (Da-Long Hu, Shao-Yong Jiang, Suo-fei Xiong, Jia-Xiang Dong, and Ke-Xin Wang) declare that they have no conflict of interest.

## References

BGMRJX (Bureau of Geology and Mineral Resources of Guangxi Province) 1984 Regional Geology of Jiangxi Province Geological Publishing House Beijing (in Chinese with English abstract)

Bischoff LJ (1991) Densities of liquids and vapors in boiling NaCl-$H_2O$ solutions; a PVTX summary from 300°C to 500°C. Amer J Sci 29:309–338

Bodnar RJ (1993) Revised equation and table for determining the freezing point depression of $H_2O$–NaCl solutions. Geochim Cosmochim Acta 57:683–684

Bodnar RJ, Lecumberri-Sanchez P, Moncada D, Steele-Macinnis M (2014) Fluid inclusions in hydrothermal ore deposits. In: Holland HD, Turekian KK (eds) Treatise on Geochemistry, 2nd edn. Elsevier Ltd, Amsterdam, pp 119–142

Bodnar RJ, Vityk MO (1994) Interpretation of microthermometric data for $H_2O$-NaCl fluid inclusions. In: Vivo BD, Frezzotti ML (eds) Fluid inclusions in Minerals, Methods and Applications. Virginia Tech, Blacksburg, pp 117–130

Campbell AR, Panter KS (1990) Comparison of fluid inclusions in coexisting (cogenetic) wolframite, Cassiterite, and quartz from St. Michael's Mount and Cligga Head, Cornwall. England Geochim Cosmochim Acta 54:673–681

Cao XF, Lü XB, He MC, Niu H, Du BF, Mei W (2009) An infrared microscope investigation of fluid inclusions in coexisting quartz and wolframite: A case study of Yaogangxian quartz-vein wolframite deposit. Mineral Deposits 28:611–620 (in Chinese with English abstract)

Charvet J (2013) The Neoproterozoic-Early Paleozoic tectonic evolution of the South China Block: An overview. J Asian Earth Sci 74:198–209

Chen J, Lu JJ, Chen WF, Wang RC, Ma DS, Zhu JC, Zhang WL, Ji JF (2008) W-Sn-Nb-Ta-bearing granites in the Nanling Range and their relationship to metallogenesis. Geol J China Univ 14:459–473 (in Chinese with English abstract)

Chen J, Wang RC, Zhu JC, Lu JJ, Ma DS (2013) Multiple-aged granitoids and related tungsten-tin mineralization in the Nanling Range, South China. Sci China Earth Sci 56:2045–2055

Chen LL, Ni P, Wang GG, Li WS, Yang YL (2018) Study on the fluid inclusion assemblages (FIA) from coexisting wolframite and quartz in Maoping tungsten deposit, southern Jiangxi province. J Nanjing Univ (natural Sci) 54:336–350 (in Chinese with English abstract)

Chi GX, Lu HZ (2008) Validation and representation of fluid inclusion microthermometric data using the fluid inclusion assemblage (FIA) concept. Acta Petrol Sin 24(9):1945–1953 (in Chinese with English abstract)

Clayton RN, Mayeda TK (1963) The use of bromine pentafluoride in the extraction of oxygen from oxides and silicates for isotopic analysis. Geochim Cosmochim Acta 27:43–52

Clayton RN, O'Neil JR, Mayeda TK (1972) Oxygen isotope exchange between quartz and water. J Geophys Res 77:3057–3067

Fan XK, Mavrogenes J, Hou ZQ, Zhang ZY, Wu XY, Dai JL (2019) Petrogenesis and metallogenic significance of multistage granites in Shimensi tungsten polymetallic deposit, Dahutang giant ore field, South China. Lithos 336–337:326–344

Fan XK, Zhang ZY, Hou ZQ, Pan XF, Zhang X, Sheng YC, Dai JL, Wu XY (2020) Mineralogical characteristics and its metallogenic implications of ore-bearing granites in the Pingmiao W-Cu deposit, Dahutang tungsten ore field. South China Acta Petrol Sin 36(12):3757–3782 in Chinese with English abstract)

Faure G (1986) Principles of Isotope Geology. John Wiley and Sons Inc, New York

Feng CY, Zhang DQ, Xiang XK, Li DX, Qu HY, Liu JN, Xiao Y (2012) Re-Os isotopic dating of molybdenite from the Dahutang tungsten deposit in northwestern Jiangxi Province and its geological implication. Acta Petrol Sin 28:3858–3868 (in Chinese with English abstract)

Gao LZ, Huang ZZ, Ding XZ, Liu YX, Pang JE, Zhang CH (2012) Zircon SHRIMP U-Pb dating of Xiushui and Majianqiao formations in northwestern Jiangxi Province. Geol Bull China 31:1086–1093 (in Chinese with English abstract)

Goldstein RH, Reynolds TJ (1994) Systematics of fluid inclusions in diagenetic minerals. Soc Sediment Geol SEPM Short Course 31:1–199

Gong XD, Yan GS, Ye TZ et al (2015) A study of ore-forming fluids in the Shimensi tungsten deposit, Dahutang tungsten polymetallic ore field, Jiangxi Province, China. Acta Geol Sin-Eng 89:822–835

Guillemette N, Williams-Jones AE (1993) Genesis of the Sb-W-Au deposits at Ixtahuacan, Guatemala: Evidence from fluid inclusions and stable isotopes. Miner Deposita 28:167–180

Hoefs J (1997) Stable Isotope Geochemistry, 4th edn. Springer-Verlag, Berlin, p 201p

Hu DL, Jiang SY (2020) In-situ elemental and boron isotopic variations of tourmaline from the Maogongdong deposit in the Dahutang W-Cu ore field of northern Jiangxi Province, South China: Insights into magmatic-hydrothermal evolution. Ore Geol Rev 122:103502

Huang LC, Jiang SY (2013) Geochronology, geochemistry and petrogenesis of the tungsten-bearing porphyritic granite in the Dahutang tungsten deposit, Jiangxi Province. Acta Petrol Sin 29:4323–4335 (in Chinese with English abstract)

Huang LC, Jiang SY (2014) Highly fractionated S-type granites from the gaint Dahutang tungsten deposit in Jiangnan Orogen, Southeast China: geochronology, petrogenesis and their relationship with W mineralization. Lithos 202–203:207–226

Jiang SY, Peng NJ, Huang LC, Xu YM, Zhan GL, Dan XH (2015) Geological characteristic and ore genesis of the giant tungsten deposits from the Dahutang ore-concentrated district in northern Jiangxi Province. Acta Petrol Sin 31:639–655 (in Chinese with English abstract)

Jiang SY, Zhao KD, Jiang H, Su HM, Xiong SF, Xiong YQ, Xu YM, Zhang W, Zhu LY (2020) Spatiotemporal distribution, geological characteristics and metallogenic mechanism of tungsten and tin deposits in China: An overview. Chin Sci Bull 65:3730–3745 (in Chinese with English abstract)

Kajiwara Y, Krouse HR (1971) Sulfur Isotope Partitioning in Metallic Sulfide Systems. Can J Earth Sci 8(11):1397–1408

Kwak TAP (1987) W-Sn skarn deposits and related metamorphic skarns and granitoids: developments in economic geology 24. Elsevier Science, Amsterdam, pp 1–468Lecumberri-Sanchez P, Vieira R, Heinrich CA, Pinto F, Wälle M (2017) Fluid-rock interaction is decisive for the formation of tungsten deposits. Geology 45:579–582

Li XH, Li WX, Li ZX, Lo CH, Wang J, Ye MF, Yang YH (2009) Amalgamation between the Yangtze and Cathaysia Blocks in South China: Constraints from SHRIMP U-Pb zircon ages, geochemistry and Nd–Hf isotopes of the Shuangxiwu volcanic rocks. Precambr Res 174:117–128

Li XH, Li ZX, Ge WC, Zhou HW, Li WX, Liu Y, Wingate MTD (2003) Neoproterozoic granitoids in South China: crustal melting above a mantle plume at ca. 825 Ma? Precambr Res 122:45–83

Lin L, Zhang GL, Yu XP (2006) Geological characteristics and oresearch prospect of Dahutang tungsten (tin) ore field in Jiangxi. Resour Surv Environ 27:25–28 (in Chinese with English abstract)

Liu YJ, Li ZL, Ma DS, Li ZL (1982) The geochemical studies of tungsten built in South China. Sci China Earth Sci 10:939–950 in Chinese with English abstract)

Lu HZ, Fan HR, Ni P, Ou GX, Shen K, Zhang WH (2004) Fluid Inclusions. Science Press, Beijing (in Chinese)

Macey P, Harris C (2006) Stable isotope and fluid inclusion evidence for the origin of the Brandberg West area Sn-W vein deposits, NW Namibia. Miner Deposita 41:671–690

Mao JW, Cheng YB, Chen MH, Pirajno F (2013) Major types and time–space distribution of Mesozoic ore deposits in South China and their geodynamic settings. Mineral Deposita 48:267–294

Mao JW, Wu SH, Song SW, Dai P, Xie GQ, Su QW, Liu P, Wang XG, Yu ZZ, Chen XY, Tang WX (2020) The world-class Jiangnan tungsten belt: Geological characteristics, metallogeny, and ore deposit model. Chin Sci Bull 65:3746–3762 (in Chinese with English abstract)

Mao ZH, Liu JJ, Mao JW, Deng J, Zhang F, Meng XY, Xiong BK, Xiang XK, Luo XH (2015) Geochronology and geochemistry of granitoids related to the giant Dahutang tungsten deposit, middle Yangtze River region, China: implications for petrogenesis, geodynamic setting, and mineralization. Gondwana Res 28:816–836

Meinert LD, Dipple GM, Nicolesku S (2005) World skarn deposits. Econ Geol 100:299–336

Ni P, Wang GG, Yu W, Chen H, Jiang LL, Wang BH, Zhang HD, Xu YF (2015a) Evidence of fluid inclusions for two stages of fluid boiling in the formation of the giant Shapinggou porphyry Mo deposit, Dabie Orogen, Central China. Ore Geol Rev 65:1078–1094

Ni P, Wang XD, Wang GG, Hunag JB, Pan JY, Wang TG (2015b) An infrared microthermometric study of fluid inclusions in coexisting quartz and wolframite from Late Mesozoic tungsten deposits in the Gannan metallogenic belt, South China. Ore Geol Rev 65:1062–1077

Ohmoto H (1972) Systematics of sulfur and carbon isotopes in hydrothermal ore deposits. Econ Geol 67:551–579

Ohmoto H (1986) Stable isotope geochemistry of ore deposits. Rev Min 6:491–559

Peng NJ, Jiang SY, Xiong SF, Pi DH (2018) Fluid evolution and ore genesis of the Dalingshang deposit, Dahutang W-Cu ore field, northern Jiangxi Province, South China. Miner Deposita 53:1079–1094

Pirajno F (2009) Hydrothermal mineral deposits. Springer, Netherlands, p 1250

Rajabpour S, Behzadi M, Jiang SY, Rasa I, Lehmann B, Ma Y (2017) Sulfide chemistry and sulfur isotope characteristics of the Cenozoic volcanic-hosted Kuh-Pang copper deposit, Saveh county, northwestern central Iran. Ore Geol Rev 86:563–583

Roedder E (1984) Fluid inclusions. Rev Min 12:644

Rollinson HR (1993) Using geochemical data: evaluation, presentation, interpretation. New York: Longman Scien—titic& Technical Essex

Ruan K, Pan JY, Cao HJ, Xiang XK, Li ZS, Shao S, Wu JJ (2015) Study on C-O-S isotopes of Shimensi tungsten deposit in Dahutang. J Min Petrol 35:57–62 (in Chinese with English abstract)

Rudnick RL, Gao S (2003) Composition of the continental crust. In: Holland HD, Turekian KK (eds) Treatise on Geochemistry, vol 3. Elsevier, pp 1–64

Schmidt C, Romer RL, Wohlgemuth-Ueberwasser CC, Appelt O (2020) Partitioning of Sn and W between granitic melt and aqueous fluid. Ore Geol Rev 117: 103263

Shmulovich KI, Landwehr D, Simon K, Heinrich W (1999) Stable isotope fractionation between liquid and vapour in water–salt systems up to 600°C. Chem Geol 157:343–354

Song WL, Yao JM, Chen HY, Sun WD, Ding JY, Xiang XK, Zuo QS, Lai CK (2018a) Mineral paragenesis, fluid inclusions, H-O isotopes and ore-forming processes of the giant Dahutang W-Cu-Mo deposit, South China. Ore Geol Rev 99:116–150

Song WL, Yao JM, Chen HY, Sun WD, Lai CK, Xiang XK, Luo XH, Fred J (2018b) A 20 m.y. long-lived successive mineralization in the giant Dahutang W-Cu-Mo deposit. South China Ore Geol Rev 95:401–407

Sun KK, Chen B (2017) Trace elements and Sr-Nd isotopes of scheelite: Implications for the W-Cu-Mo polymetallic mineralization of the Shimensi deposit, South China. Am Min 102:1114–1128

Sun KK, Chen B, Deng J, Ma XH (2018) Source of copper in the giant Shimensi W-Cu-Mo polymetallic deposit, South China: Constraints from chalcopyrite geochemistry and oxygen fugacity of ore-related granites. Ore Geol Rev 101:919–935

Taylor BE (1986) Magmatic volatiles: Isotopic variation of C, H, and S. Rev Mineral 16:185–226

Wei WF, Shen NP, Yan B, Lai CK, Yang JH, Gao W, Liang F (2018) Petrogenesis of ore-forming granites with implications for W-mineralization in the super-large Shimensi tungsten-dominated polymetallic deposit in northern Jiangxi Province, South China. Ore Geol Rev 95:1123–1139

Xia QL, Wang XQ, Liu ZZ (2018) Tungsten metallogenic and geological features and mineral resource potential in China. Earth Sci Front 25:50–58 (in Chinese with English abstract)

Xiang XK, Liu XM, Zhan GN (2012) Discovery of Shimensi superlarge tungsten deposit and its prospecting significance in Dahutang area, Jiangxi Province. Resour Surv Environ 33:141–151 (in Chinese with English abstract)

Xiang XK, Wang P, Sun DM, Zhong B (2013) Isotopic geochemical characteristics of the Shimensi tungsten-polymetallic deposit in northern Jiangxi province. Acta Geosci Sin 34:263–271 (in Chinese with English abstract)

Xiong SF, Gong YJ, Yao SZ, Shen CB, Ge X, Jiang SY (2017) Nature and evolution of the ore-forming fluids from Nanmushu carbonate-hosted Zn-Pb deposit in the Mayuan District, Shaanxi Province, Southwest China. Geofluids 5:1–19

Ye ZH, Wang P, Xiang XK, Yan Q, Li YK, Guo JH (2017) Early cretaceous tungsten mineralization in southeastern China: the Wuning example. Int Geol Rev 59:946–964

Zhang LG, Liu JX, Chen ZS, Zhou HB (1994) Experimental investigations of oxygen isotope fractionation in cassiterite and wolframite. Econ Geol 89:150–157

Zhang MY, Feng CY, Wu G, Wang H, Wu Y, Han MM, Wu WH (2018) Fluid inclusion study and stable isotope characteristics of the Kunshan W-Mo-Cu deposit in the Dahutang area, northern Jiangxi Province, China. Acta Petrol Sin 34:2615–2631 (in Chinese with English abstract)

Zhang ZY, Hou ZQ, Peng HM, Fan XK, Wu XH, Dai JL (2019) In situ oxygen isotope, trace element, and fluid inclusion evidence for a primary magmatic fluid origin for the shell-shaped pegmatoid zone within the giant Dahutang tungsten deposit, Jiangxi Province, South China. Ore Geol Rev 104:540–560

Zhou XM, Sun T, Shen WZ, Shu LS, Niu YL (2006) Petrogenesis of Mesozoic granitoids and volcanic rocks in South China: a response to tectonic evolution. Episodes 29:26–33

Zhou TF, Yue SC, Yuan F (2001) H, O isotope geochemistry and transport-reaction dynamic processes of ore-forming fluid for Cu, Au deposits in the Yueshan orefield. Anhui Province Geol Anhui 11(2):131–139

Zhu ZY, Cook NJ, Yang T, Ciobanu CL, Zhao KD, Jiang SY (2016) Mapping of sulfur isotopes and trace elements in sulfides by LA-(MC)-ICP-MS: potential analytical problems, improvements and implications. Fortschr Mineral 6:110

Zhu ZY, Jiang SY, Ciobanu CL, Yang T, Cook NJ (2017) Sulfur isotope fractionation in pyrite during laser ablation: implications for laser ablation multiple collector inductively coupled plasma mass spectrometry mapping. Chem Geol 450:223–234

Zuo QS, Zhang P, Zhou CJ (2014) Basic characteristics of Yanshanian magmatic rocks and its implication for mineralization in Dahutang ore-concentrated area of Jiangxi. Min Resour Geol 28:519–526 (in Chinese with English abstract)